Supplemental Material

Glutamyl-prolyl-tRNA Synthetase Regulates Proline-rich Pro-fibrotic Protein Synthesis during Cardiac Fibrosis

Jiangbin Wu, Kadiam C Venkata Subbaiah, Li Huitong Xie, Feng Jiang, Eng-Soon Khor, Deanne Mickelsen, Jason R Myers, Wai Hong Wilson Tang, Peng Yao

Expanded Materials & Methods

Reagents, antibodies and siRNAs

Halofuginone hydrochloride (Halo) was purchased from Santa Cruz Biotechnology (sc-211579). Isoprenaline (ISO), cycloheximide (CHX), and Leucinol were purchased from Sigma-Aldrich. The siRNAs against mouse Sulf1 (assay ID: s109342 and s109343) and negative control siRNA were obtained from ThermoFisher Scientific and transfected into cardiac fibroblasts by lipofectamine 3000 (ThermoFisher) following the instruction manual.

Primary antibodies used in this study include: rabbit polyclonal anti-SULF1 (PA5-50890), anti-Collagen III (PA527828), anti-Periostin (PA5-34641) and mouse monoclonal anti-Myh6 (Ma5-27819) antibodies were purchased from ThermoFisher Scientific. Mouse monoclonal anti-COL1A1 (SAB1402151-100UG), anti-FLAG tag M2 (F1804), anti-α-Actinin (A7811), and anti-α-smooth muscle actin (A2547) antibodies were purchased from Sigma-Aldrich. Mouse monoclonal anti-COL3A1 (sc-271249), anti-ProRS (sc-393505), and anti-CysRS (sc-390230) antibodies were purchased from Santa Cruz Biotechnology. Mouse monoclonal anti-GAPDH (60004-1-Ig), rabbit polyclonal anti-FLAG tag (20543-1-AP), and anti-Vimentin (10366-1-AP) antibodies were purchased from ProteinTech. The rabbit polyclonal anti-EPRS (ab157122) antibody was purchased from Abcam. The overexpression vector and lentivirus (titer >10^8 TU/ml) of mSULF1-FLAG (VB191007-1166ekk) and mEPRS-FLAG (VB191007-1162bxu) were purchased from VectorBuilder.

Human specimens

All human samples of frozen cardiac tissues, including 17 samples from explanted failing hearts and 8 samples from non-failing donor hearts, as well as paraffin section slides from DCM, ISHF or non-failing hearts were acquired from the Cleveland Clinic. This study was approved by Material Transfer Agreement between the URMC and the Cleveland Clinic. All human samples were picked

up randomly based on the presence or absence of heart failure by our collaborator, Dr. Wai Hong Wilson Tang at Cleveland Clinic. We are blinded from any clinical data. There may still be some sort of bias in the inclusion of human samples as exemplified as follows: 1) the sample size is limited and it may not fully reflect the outcome from a much larger population. 2) a sub-region of the left ventricle of the human hearts were collected for the experiments. Thus, it may not fully recapitulate the outcome in the whole heart. This is a limitation within human samples experiments in the current research. In Figure 1B, total RNA samples from two non-failing donor hearts showed degradation during the quality control process and were excluded from RT-qPCR analysis.

Generation of *Eprs* global knockout mice

Eprs global knockout (gKO) mouse was generated by the Mouse Genome Editing Resource at URMC. The guide RNA (gRNA) used for *Eprs* KO was designed using a CRISPR RNA online design tool developed by Dr. Feng Zhang's lab (http://crispr.mit.edu). The gRNA with highest score and lowest off-target probability was chosen. The efficiency of gRNA and Cas9-2xNLS (Synthego) were tested in a tube *in vitro* using a 500-bp mouse genomic DNA-derived PCR product that contains the target sequence. Then, 25 pmol of single guide RNA (sgRNA) and 25 pmol of Cas9 nuclease were mixed in the injection buffer in a total of 12.5 μl reaction. The mixture was then incubated at room temperature (RT) for 10 mins to form the RNP complex. Finally, this RNP complex was mixed with a single strand DNA template that contains two consecutive stop codons followed by an additional frame-shifting adenosine nucleotide (UAAUAAA) in frame of *Eprs* at 1:3 molar ratio for pronuclear injection. In this project, 148 injected embryos were transferred into 4 recipient C57/BL6J mice and finally we obtained 2 mosaic pups containing premature stop codons in the exon 3 of *Eprs*. In order to get the heterozygous gKO mice for experiments, 2 mice from injection were bred with C57BL/6J WT mice for germline transmission and kept breeding with WT mice for 5 generations to remove the potential off-target sites. The genotyping primer set (Online Table XI) for the *Eprs* gKO mice was designed to complement with the mutated nucleotides of the protospacer adjacent motif (PAM) sequence. There is a 470-bp PCR amplification product from the mutant allele but no amplification from the WT allele.

Guide RNA (23-nt): 5'-GCUAGAAUUGCAACUACGUCUGG-3'

DNA template (157-nt): 5'-GTTTACATAATGCTTCAATTCTAGG ACT GTG GCA TTC ACT GAC GTG AAT TCA ATC CTG CGC TAC CTG GCT AGA ATT GCA ACT ACG TAA TAA A TCT CAG CTG TAT GGG ACT AAC CTG ATG GAG CAC ACT GAGGTAAGCGAGGAGTATTTCTTTTCCT-3'

Generation of tamoxifen-inducible Postn-Cre-driven *Eprs* conditional knockout mice

Eprs conditional knockout (cKO) mouse line *Eprs*_tm1c_B03 (C57BL6/N-Eprs<tm1c(EUBOMM)Hmgu>/Tcp) was purchased from The Center for Phenogenomics (TCP, Toronto, Canada) in the form of frozen sperms. The *Eprs*$^{flox/+}$ tm1c cKO mouse line was rederived using *In Vitro* Fertilization (IVF) performed by the Mouse Genome Editing Resource at URMC. The *Eprs* cKO tm1c mouse line was bred with *Postn*$^{MCM/+}$ mice to obtain tamoxifen-inducible *Postn*-Cre-driven *Eprs*$^{flox/+}$ tm1d cKO mouse line. We used one single initial dose of 30 μg/g of mouse body weight for tamoxifen (TMX) intraperitoneal injection followed by TMX food for the entire pathological stimulus of TAC surgery.

Mouse heart failure models

In this study, we used three mouse heart failure models, including ISO osmotic minipump implantation, transverse aortic constriction (TAC), and left anterior descending coronary artery ligation (LAD ligation)/myocardial infarction (MI) surgical models. Experimental mice are siblings generated from intercrosses between *Eprs*$^{+/-}$ and C57BL/6J WT mice. Age and background matched WT and *Eprs*$^{+/-}$ male mice at the age of 8-12 weeks were used for most of the mouse studies. All the minipump implantation and surgeries were performed by the Mouse Microsurgical Core as previously described.

For the osmotic minipump implantation, mice were anesthetized using 2.0% isoflurane and placed on a heated surgical board. A side/upper back area skin incision was made, and the mini-osmotic pump was inserted subcutaneously and set to deliver ISO (or vehicle) at a rate of 20 mg/Kg/day. The incision was then closed with 6-0 coated vicryl in a subcuticular manner, and the animals were allowed to recover. The sutures were removed after 2 weeks since the pumps were transplanted. The pumps were not removed and remained for a time period of 4 weeks. The animals were euthanized after 4 weeks of ISO infusion and mouse hearts were harvested for experiments, including RNA, protein extraction and sectioning.

For the TAC surgery, mice were anesthetized via continuous administration of inhaled isofluorane (2.0%) while surgery was performed. The animals were placed supine, and a midline cervical incision was made to expose the trachea for direct intubation with 22-gauge plastic catheter. The catheter was connected to a volume-cycled ventilator supplying supportive oxygen. A right thoracotomy was performed. Stenosis was induced using a 27-gauge needle placed on the ascending aorta. Sham-operated mice underwent all aspects of the surgery besides the actual aortic ligature. A ligature was made around the needle and the aorta, completely occluding the

aorta. The needle was then removed, causing severe aortic stenosis. Echocardiographic image collection was performed using a Vevo2100 echocardiography machine (VisualSonics, Toronto, Canada) and a linear-array 40 MHz transducer (MS-550D). Heart rate was monitored during echocardiography measurement. The stenotic gradient pressure was calculated to evaluate the efficacy of TAC. Left ventricular end-diastolic diameter (LVEDD), left ventricular end-systolic diameter (LVESD), wall thickness of left ventricular anterior (LVAWT) and posterior (LVPWT), ejection fraction (EF), and fractional shortening (FS) were assessed. For the intervention model of TAC surgery in conditional KO mice, the TAC surgery was performed and tamoxifen diet was fed for another 6 weeks 14 days post TAC surgery after single initial dose of tamoxifen at 30 μg/g of mouse body weight of intraperitoneal injection. In Figure 2H, one separate batch of WT Sham mice were used for echocardiography analysis to test the variability.

The LAD ligation-based MI surgery was performed as previous described by the Mouse Microsurgical Core of Aab CVRI. For the MI model in Online Figure III, female mice were used. For our standard MI procedure, mice are placed on a heating pad and the airway stabilized by endotracheal intubation and mechanical ventilation provided (inspiratory tidal volume of 250 μL at 130 breaths/min). The mice were given Buprenorphine 2.5 mg/Kg via subcutaneous injection. Maintenance anesthesia is typically 1.5% isoflurane by inhalation. A midline cervical incision was made to expose the trachea for intubation with a PE90 plastic catheter. The catheter was connected to a Harvard minivent supplying supplemental oxygen with a tide volume of 225-250 μl and a respiratory rate of 130 strokes/min. Surgical plane anesthesia was subsequently maintained at 1-1.5% isoflurane. Skin was incised and chest cavity opened at the level of the 4^{th} intercostal space. Oral intubation was employed by placing PE 90 tubing in the mouth and advancing slowly into the trachea. Mechanical P.I. ventilation (tidal volume of approximately 0.4 ml at 130 breaths/min) was then begun. After intubation, a midline incision was made between the sternum and the left internal mammalian artery. Alternatively, a lateral incision (left thoracotomy) was made in the 4^{th} intercostal space. The mouse heart was exposed and the left coronary artery branch points are visualized under 10x magnification prior to ligation, and the LAD coronary artery ligated intramurally 2 mm from its ostial origin for standard MI with a 9-0 proline suture. Transmural ischemia is assured by color loss on the left ventricle wall and ST-segment elevation noted on the electrocardiogram. Lungs were reinflated and the chest was closed in two layers; the ribs (inner layer) were closed with 6-0 coated vicryl sutures in an interrupted pattern. The skin was closed using 6-0 nylon or silk sutures in a subcuticular manner. The anesthesia was stopped and once the mouse was breathing on its own, the mouse was removed from the ventilator and allowed to

recover in a clean cage on a heated pad. A sham operation is performed using the same procedure, but a suture is passed under the LAD coronary artery without ligation.

The mice are randomized for experiments using simple randomization with a specific ID number before animal procedures. Animal operations, including ISO infusion, TAC surgery, MI surgery, and echocardiography measurement, were performed by the Microsurgical Core surgeons. Sections and histology analysis were done by the Histology Core. The technicians from both Microsurgical Core and Histology Core were all blinded to the genotypes of the mice and tissue samples. For group size justification, we performed the power analysis using both G*power version 3.1.9.6 and the function of power.anova.test in R version 3.5.3 (R Foundation for Statistical Computing, Vienna, Austria). The assumptions of our power calculations include the same standard variance in each study group, effect size=$\frac{\text{Difference of the means between study groups}}{\text{common standard deviation}}$, alpha level=0.05, power=0.9 and number of study groups. The effect size for specific experiments is assumed based on previous similar studies or literature. In previous experiences from our Microsurgical Core, we have observed a survival rate of ~90% after the TAC procedure. To offset the possible loss of mice per treatment, we added at least one mouse per treatment group.

Adult cardiomyocyte and cardiac fibroblast isolation

Langendorff perfusion system was used to isolate adult cardiomyocytes (CMs) and cardiac fibroblasts from the murine heart. Mice were fully anesthetized via intraperitoneal injection of ketamine/xylazine. Once losing pedal reflex, the mouse was secured in a supine position. The heart was excised and fastened onto the CM perfusion apparatus and perfusion was initiated in the Langendorff mode. Our Langendorff perfusion and digestion consisted of three steps at 37°C: 4 mins with perfusion buffer (0.6 mM KH_2PO_4, 0.6 mM Na_2HPO_4, 10 mM HEPES, 14.7 mM KCl, 1.2 mM $MgSO_4$, 120.3 mM NaCl, 4.6 mM $NaHCO_3$, 30 mM taurine, 5.5 mM glucose, and 10 mM 2,3-butanedione monoxime), then switched to digestion buffer (300 U/ml collagenase II [Worthington] in perfusion buffer) for 3 mins, and finally perfused with digestion buffer supplemented with 40 μM $CaCl_2$ for 8 mins. After perfusion, the ventricle was placed in sterile 35 mm dish with 2.5 ml digestion buffer and shredded into several pieces with forceps. 5 ml stopping buffer (10% FBS, 12.5 μM $CaCl_2$ in perfusion buffer) was added and pipetted several times until tissues disperse readily, and solution turned cloudy. The cell solution was passed through 100 μm strainer. CMs were settled by incubating the cell suspension at 37°C for 30 mins. The CMs were resuspended in 10 ml stopping buffer and subjected to several steps of calcium ramping: 100 μM $CaCl_2$, 2 mins; 500 μM $CaCl_2$, 4 mins; 1.4 mM $CaCl_2$, 7 mins. Then the CMs were seeded

onto a glass bottom dish (Nest Biotechnology) pre-coated with laminin (ThermoFisher Scientific). Plates were centrifuged for 5 mins at 1,000 g at 4°C to increase the adherence, cultured at 37°C for ~1 hr, and then switched to CM media (MEM [Corning] with 0.2% BSA, 10 mM HEPES, 4 mM $NaHCO_3$, 10 mM creatine monohydrate, 1% penicillin/streptomycin, 0.5% insulin-selenium-transferrin and blebbistatin) for cell culture and further treatments.

Cardiac fibroblasts (CFs) from the supernatant are pelleted for 5 mins at 1,000 rpm at 4°C. CFs were plated in 4-5 ml CF media (DMEM with 10% FBS and 1% penicillin/streptomycin) in 60 mm plate and washed vigorously 3-5 times with 2 ml 1x PBS after 2-3 hrs, and replaced with fresh CF media. For CF only isolation, pre-weened mice were fully anesthetized and the heart was directly cut into small pieces and digested in the digestion buffer for 4x 10 mins at 37°C with slow stirring and CFs were plated the same as Langendorff isolation of CFs.

Cell culture

NIH/3T3 cells were cultured in DMEM supplemented with 10% bovine calf serum (VWR) and 1% penicillin/streptomycin (ThermoFisher). For halofuginone treatment, NIH/3T3 cells were grown to ~60-70% confluency and treated with 100 nM halofuginone or vehicle, or at the concentration as indicated for 24 hrs. Primary CFs isolated from mouse hearts were cultured in DMEM supplemented with 10% FBS (ThermoFisher) and 1% penicillin/streptomycin. Primary cells were used before P2 generation for polysome profiling and at P0 for CF activation assays. siRNA transfection (100 nM) in primary CFs was performed using lipofectamine 3000 following the manufacturer's instructions.

Polysome profiling

Polysome profiling was performed to measure the global cytosolic translational status or the translational efficiency of specific genes in both NIH/3T3 cells and primary CFs. Briefly, after drug treatment of cells (Halo, ISO or vehicle), cycloheximide (CHX, Sigma) was added to the cells at a final concentration of 100 μg/ml for 15 mins before lysis to freeze ribosomes on mRNAs. ~5 X 10^6 cells were lysed in TMK lysis buffer (10 mM Tris-HCl pH 7.4, 5 mM $MgCl_2$, 100 mM KCl, 1% Triton X-100, 0.5% Deoxycholate, 2 mM DTT) containing 100 μg/ml CHX, 4 U/ml RNase inhibitor (NEB), and proteinase inhibitor cocktail (Roche) on ice for 15 mins. Equal amounts of A_{260} absorbance from each sample were loaded onto a 10-50% sucrose gradient solution, and centrifuged at 29,000 rpm for 4 hrs at 4°C. The polysome fractions were collected from each sample by a density gradient fractionation system (BRANDEL). For specific genes, total RNA was extracted from the same volume of each fraction with Trizol LS (ThermoFisher) and used for RT-

qPCR. Based on the UV absorbance curve, the 22 fractions were pooled into 7 samples for RT-qPCR analysis including free mRNP (fraction 1), 40S small ribosome subunit (fraction 2), 60S large ribosome subunit (fraction 3), 80S monosome (fraction 4), light polysomes (disome, trisome, etc.; fraction 5 and 6), and heavy polysomes (>5 ribosomes; fraction 7). *In vitro* transcribed renilla luciferase mRNA was used as a spike-in control for normalization. For polysome-Seq, all the fractions were pooled into 3 samples, polysome free (free mRNP, 40S subunit, 60S subunit), light polysomes (monosome, disome, trisome, tetrasome), and heavy polysomes (≥5 ribosomes). Total RNAs were extracted from the same volume of 3 samples and subjected to RNA-Seq. The RNA-Seq and polysome-Seq data were uploaded to NCBI GEO database with ID of GSE136838.

mRNA expression detection by quantitative PCR

For heart tissues (human and mouse) or cell samples, the RNA extraction was performed using TRIzol reagent (ThermoFisher) following instructions in the manual and used for the detection of the expression of specific genes. Briefly, the tissues were homogenized in TRIzol using Minilys Personal Homogenizer (Bertin Technologies) and placed on ice for 15 mins to lyse the tissue. For the polysome fraction samples, total RNA extraction was performed using TRIzol LS reagent at a volume ratio of 1:3 following the manual. The *in vitro* transcribed renilla luciferase mRNA was added to the samples before RNA extraction as a spike-in loading control.

For the mRNA detection, 1 μg of total RNA was used as a template for reverse transcription using the iScript cDNA Synthesis Kit (Bio-Rad). cDNA was used for detecting the expression of Eprs, Sulf1, Ltbp2, and the marker genes, Nppa, Nppb, Col1a1 and Col3a1. 18S rRNA or Gapdh was used as a normalization control for mRNA expression. The SYBR Green primer sequences or the Taqman probes were listed in Online Table XI. All the primers showing only one peak in melting curve were used in this study. qPCR procedure: 1) initial denaturation at 95°C for 60 sec. 2) 40 cycles of denaturation at 95°C for 10 sec and annealing/extension at 60°C for 45 sec. 3) melt curve analysis by 0.5°C increments at 5 sec/step between 65-95°C.

RNA-Seq and polysome-Seq NGS data processing, alignment and analysis

Total RNA extracted from halofuginone or vehicle treated NIH/3T3 cells or polysome fractions were treated with DNase I (NEB) to remove potential genomic DNA in the RNA samples. The DNase I treated RNA samples were purified with phenol:chloroform:isoamyl alcohol and then subjected to RNA-Seq at the Genomic Research Center of URMC. Raw reads generated from the Illumina HiSeq2500 sequencer were demultiplexed using bcl2fastq version 2.19.0. Quality filtering and adapter removal are performed using Trimmomatic version 0.36[23] with the following

parameters: "TRAILING:13 LEADING:13 ILLUMINACLIP: adapters.fasta:2:30:10 SLIDINGWINDOW:4:20 MINLEN:15". Processed/cleaned reads were then mapped to the *Mus musculus* reference genome (GRCm38, mg38) with STAR_2.5.2b[24] given the following parameters: "—twopassMode Basic --runMode alignReads --genomeDir ${GENOME} --readFilesIn ${SAMPLE} --outSAMtype BAM SortedByCoordinate --outSAMstrandField intronMotif --outFilterIntronMotifs RemoveNoncanonical". The subread-1.5.0[25] package (featureCounts) was used to derive gene counts given the following parameters: "-s 2 -t exon -g gene_name" and the gencode M12 gene annotations. Differential expression analysis and data normalization was performed using DESeq2-1.16.1[26] with an adjusted p-value threshold of 0.05 within an R-3.4.1[27] environment. The p_{adj} (p-value adjusted, or false discovery rate FDR) is the p-values adjusted for multiple testing with correction using the Benjamini-Hochberg procedure. Follow-up biochemical and cellular experiments were done to confirm the true positive and exclude possible false positive hits from the large-scale screen. A batch factor was given to the differential expression model in order to control for batch differences. Gene ontology of Biological Process (Figure 6B) and KEGG pathway enrichment (Figure 5E and Online Figure VIIF) analyses were performed using DAVID Bioinformatics Resources 6.8[34].

Proline motif analysis across mouse and human proteomes

The proteomic sequences of UniProtKB/Swiss-Prot reviewed proteins of Homo sapiens (UP000005640, reviewed, 20,328 sequences) and Mus musculus (UP000000589, reviewed, 16,966 sequences) were downloaded from Uniprot database (https://www.uniprot.org/) in fasta format. Each protein sequence was processed and the number of consecutive prolines (PP, PPP, PPPP, P…P_n [n=2-9, and n≥10], etc.) motifs were calculated using R package "Biostrings" (R version 3.3.3). The number of consecutive proline motifs were quantified. Briefly, the consecutive proline motifs were counted without any overlapping and the number of PP or PPP within protein containing higher number of consecutive proline (more than 2 or 3 for PP or PPP) was determined by the whole number after division of the consecutive proline length by 2 (PP) or 3 (PPP). For example, the 4 and 5 consecutive proline stretch will be considered as 2 PP motifs and 1 PPP motifs while 6 and 7 consecutive proline stretch as 3 PP motifs and 2 PPP motifs. The conserved PP motif containing genes were generated by overlapping the PP motif containing genes in human and mouse proteomes.

Cardiac fibroblasts activation assay

Adult CF cells were isolated from hearts of 2-3 months old and pre-weened mice and seeded into 35 mm glass bottom dishes. After attachment for 2 hrs, the cells were washed with PBS for 3 times,

replaced with fresh CF growth media (DMEM supplemented with 10% FBS and 1% penicillin/streptomycin), and cultured at 37°C overnight. On the second day, 100 nM of Sulf1 siRNAs or control siRNAs were transfected using lipofectamine 3000 following the manual. The cells were cultured for additional 36 hrs and 10 ng/ml recombinant mouse TGFβ1 (ThermoFisher) was added to the media for 24 hrs following a 12 hr serum starvation. Then the cells were fixed with 4% paraformaldehyde (PFA) for immunofluorescence or lysed in TRIzol reagent for the marker gene detection by RT-qPCR. In order to measure the collagen production in myofibroblasts, adult CF cells were treated with 10 ng/ml TGF-β for 24 hrs to activate the cardiac fibroblast, and then cultured with 100 nM Halo or vehicle for additional 24 hrs. The activated myofibroblasts were fixed with 4% PFA for immunofluorescence.

Immunofluorescence and immunohistochemistry

For the immunofluorescence (IF), the primary CF cells were fixed using 4% PFA/PBS and washed with PBS for 3x 5 min. The cells were permeabilized by ice-cold 0.5% triton X-100/PBS for 5 mins and washed with PBS for 3x 5 min. After blocking with 4% BSA in PBS for 30 mins, the cells were incubated with indicated primary antibodies (rabbit anti-SULF1, 1:200; mouse anti-α-SMA, 1:500; mouse anti-COL1A1, 1:200; rabbit anti-Periostin, 1:300; rabbit anti-COL3A1, 1:200; mouse and rabbit anti-FLAG, 1:250) in blocking solution (4% BSA in PBS) overnight at 4°C, and washed with PBS for 3x 5 min. Then, the cells were co-stained with the Alex Fluor-488 and Alex Fluor-594 conjugated secondary antibodies (ThermoFisher, 1:250) in blocking solution for 45 mins and washed with PBS for 3x 5 min. Finally, the cells were co-stained with DAPI for 5 mins and kept in PBS buffer inside before imaging.

For the immunohistochemistry (IHC), the mouse heart tissues were fixed with 10% neutralized formalin solution and processed for paraffin embedded sections in the Histological Core of Aab CVRI. For paraffin embedded sections from both human and mouse hearts, the sections were deparaffinized by the following steps: xylene (100%) for 2x 5 min; ethanol (100%) for 2x 5 min; ethanol (95%) for 1x 5 min; ddH_2O for 2x 5 min. Antigen retrieval was performed by boiling the deparaffinized section in 10 mM citrate buffer, pH 6.0 and auto-fluorescence was quenched by incubation in 3% H_2O_2/PBS for 30 mins at RT. Then the slides were incubated with blocking buffer (5% goat serum in PBS) for 1 hr at RT and the indicated primary antibody (rabbit anti-SULF1, 1:200; mouse anti-α-SMA, 1:500; mouse anti-COL1A1, 1:200; mouse and rabbit anti-EPRS, 1:300; mouse anti-α-Actinin, 1:500; rabbit anti-Vimentin, 1:250; mouse anti-Myh6, 1:300) in blocking solution overnight at 4°C. Alex Fluor-488 and Alex Fluor-594 conjugated secondary antibodies were incubated for 1 hr following 3x 5 min washing step. Finally, the slides were co-

stained with DAPI in the mounting media and covered by coverslips. The images were taken using an Olympus FV1000 confocal microscope and the intensity was measured by NIH Image J software.

A negative control using the same amount of secondary antibody only was performed for IF or IHC to confirm the fluorescence signals as genuine target staining signals and not non-specific background. The specificity of primary antibodies were confirmed in other ways. ThermoFisher company has confirmed the specificity of Periostin (POSTN) antibody (PA5-34641) using shRNA knockdown followed by Western blotting. We confirmed the specificity of SULF1 antibody (PA5-50890) by siRNA knockdown in cultured cardiac fibroblasts and observed significant decrease in IF signals (Online Figure XA). The specificity of EPRS antibody (ab157122) was supported by ~50% reduction of IF signals in heart tissue sections from WT and *Eprs*$^{+/-}$ mice (Online Figure IIE and IIF) and IB signals of Western blotting using heart lysates (Online Figure IID). For the COL1A1 antibody (SAB1402151-100UG), the IF signal was drastically induced by TGF-β treatment (Figure 4E and Online Figure XC) and the IB signal was significantly reduced by Halo treatment (Figure 8D). These observations confirmed the specificity of antibodies used in this research.

Wheat germ agglutinin (WGA) and phalloidin staining

WGA staining was used to quantify the size of CMs in the murine heart after drug treatments. Deparaffinization, antigen retrieval and quenching of auto-fluorescence were performed the same as described above. The section dots were marked by Dako pen and stained with 10 μg/ml WGA-Alex Fluor-488 (ThermoFisher) for 1.5 hr at RT. Then the slides were washed with PBS for 3x 5 min. The slides were covered by coverslips with antifade solution (containing DAPI) for imaging. The images were taken in the fluorescence microscope and Image J software was used to quantify the cell size of CMs.

Primary CMs were isolated from WT (*Eprs*$^{+/+}$) and *Eprs*$^{+/-}$ mice and treated with vehicle or ISO for 24 hrs. Cultured myocytes were fixed using 4% PFA, washed with PBS, and permeabilized in 0.5% Triton X-100. Alexa Fluor^{TM} 594 Phalloidin (ThermoFisher, Cat. No. A12381) was used to stain the skeleton actin protein for 30 mins at RT. The stained cells were gently washed with PBS for 3x 5 min and mounted using anti-fade mounting medium with DAPI (Vector). The images were taken in the fluorescence microscope and Image J software was used to quantify the cell size of CMs.

Picrosirius red staining

Picrosirius red staining was performed to measure the cardiac fibrosis in heart failure models

using picrosirius red solution (Abcam) following the manufacturer's instruction. Briefly, paraffin embedded tissue sections were deparaffinized and incubated in picrosirius red solution at RT for 1 hr. Then, slides were subjected to 2 washes of 1% acetic acid and 100% of ethyl alcohol, and mounted in a mounting medium. Images were captured using the PrimeHisto XE Histology Slide Scanner (Carolina) and cardiac fibrotic area was quantified from the whole heart images of picrosirius red staining using Image J software. Due to unexpected occasional tissue block and section damage, some animal samples had to be eliminated in one specific case. In Figure 2F, *Eprs*$^{+/-}$ Sham=8, *Eprs*$^{+/-}$ TAC=6.

Statistical analysis

All quantitative data were presented as mean ± SEM and analyzed using Prism 8.3.0 software (GraphPad). The statistical significance was analyzed by Prism 8.3.0 and R 3.5.1, and the non-parametric post hoc pairwise comparisons were performed using r package PMCMR. We used Kolmogorov-Smirnov test to assess if the data are normally distributed (N≥10), and parametric tests (unpaired student t test or ANOVA for normally distributed data) or non-parametric tests (unpaired Mann-Whitney test or Kruskal-Wallis test for not normally distributed data) were used accordingly. Since the normality cannot be assessed on the data with small sample size (N<10), we performed non-parametric tests across our data with small sample size (N<10). For comparison between 2 groups, non-parametric unpaired Mann-Whitney test was performed. For comparisons among ≥3 groups, non-parametric Kruskal-Wallis test was performed with Conover-Iman method for post hoc pairwise comparisons and Benjamini-Hochberg method for type I error correction. For the counts of proline-rich genes, chi-square (χ^2) test was performed. Two-sided *P* values <0.05 were considered to indicate statistical significance. Overall *P* values for comparisons among ≥3 groups were provided in the Supplemental File. Specific statistical methods and post hoc tests were described in the figure legends.

Online Figure Legends

Online Figure I. Upregulation of EPRS in TGF-β activated human cardiac fibroblasts.

(A) Transcriptional activation of cytosolic ARSs, including EPRS in TGF-β stimulated human CFs.

(B) No remarkable transcriptional activation of other translation factors in TGF-β stimulated human CFs. Abbreviations: eIF; eukaryotic initiation factor; eEF: eukaryotic elongation factor; eTF: eukaryotic termination factor.

Online Figure II. Generation and characterization of *Eprs*$^{+/-}$ heterozygous knockout mice.

(A) Schematic of the generation of *Eprs*$^{+/-}$ mice by CRISPR technology.

(B) Sanger DNA sequencing confirms an insertion of two tandem stop codons in *Eprs* knockout allele.

(C) Genotyping of *Eprs*$^{+/+}$ and *Eprs*$^{+/-}$ mice.

(D) *Eprs* mRNA and protein expression are reduced by ~50% in *Eprs*$^{+/-}$ mouse hearts. n=4, two male and two female mice were used.

(E) Immunostaining shows EPRS is reduced by ~50% in Vimentin positive CFs in *Eprs*$^{+/-}$ mice**.** Scale bar: 50 μm. Quantification of EPRS intensity is shown for n>200 cells from three murine hearts.

(F) Immunostaining shows EPRS is reduced by ~50% in α-actinin positive CMs in *Eprs*$^{+/-}$ mice**.** Quantification of EPRS intensity is shown. Scale bar: 50 μm. Quantification of EPRS intensity is shown for n>200 cells from three murine hearts.

(G) Phalloidin staining of ISO-treated primary mouse CMs isolated from WT and *Eprs*$^{+/-}$ mice. 10 μM ISO was used for the treatment. Scale bar: 100 μm. Quantification of cell sizes is shown for n>500 cells from three replicated experiments.

Comparisons were performed by non-parametric unpaired Mann-Whitney test for D-F, and Kruskal-Wallis test with Conover-Iman method for post hoc pairwise comparisons and Benjamini-Hochberg correction for G.

Online Figure III. *Eprs* haploinsufficiency reduces cardiac fibrosis in the MI surgery model.

(A-B) Picrosirius staining was performed in a series of six heart tissue sections from apex to base and fibrotic area was quantitatively measured. N=4-6. Scale bar: 2 mm.

Comparisons were performed by non-parametric Kruskal-Wallis test with Conover-Iman method for post hoc pairwise comparisons and Benjamini-Hochberg correction for B.

Online Figure IV. Generation and characterization of *Eprs* conditional knockout mice.

(A) Breeding strategy for generating tamoxifen-inducible Postn-Cre-driven *Eprs* conditional KO mice.

(B) Genotyping of *Eprs* conditional KO mice.

(C) EPRS is reduced by ~45% in α-SMA positive myofibroblasts in *Eprs* cKO mice under TAC surgical conditions indicated by immunofluorescence**.** Quantification of EPRS intensity is shown. Scale bar: 50 μm. N>200 cells from three hearts. Comparisons were performed by non-parametric unpaired Mann-Whitney test.

Online Figure V. The effect of EPRS overexpression and knockdown on collagen protein expression in cardiac fibroblasts.

(A) EPRS expression does not positively correlate with CM hypertrophy marker gene expression in human heart samples. Pearson correlation coefficient was presented.

(B) *Eprs* mRNA is induced by pro-hypertrophic and pro-fibrotic agonists in primary mouse CFs. ISO: 10 μM; Ang II: 200 nM; TGF-β: 10 ng/ml; IL-11: 5 ng/ml.

(C) ISO-induced EPRS mRNA and protein expression in primary mouse CFs. 18S rRNA and GAPDH are used for loading controls for mRNA (n=6) and protein (n=4) quantification, respectively.

(D) Myofibroblast marker gene mRNA expression is strongly induced by TGF-β, but not ISO in primary mouse CFs.

(E) Left panel: Collagen mRNA expression is slightly increased in ISO-treated primary mouse CFs (n=6). 18S rRNA is used as a loading control. Middle panel: Representative Western blot images from two biological replicates indicate that collagen proteins are strongly induced by ISO in primary mouse CFs. Right panel: The protein/mRNA ratio of collagen genes is strongly increased in ISO-treated primary mouse CFs. The protein/mRNA ratio was calculated by pair-wise comparison of quantification of two biological replicates of Western blot with six biological replicates of mRNA expression.

(F) Upper panel: Polysome-RT-qPCR assay indicates that EPRS inhibition by Halo reverses ISO-induced polysome association with *Col3a1* mRNA in primary mouse CFs. Low panel: Polysome-associated *Col3a1* mRNA is reduced in primary *Eprs*$^{+/-}$ CFs compared to WT (*Eprs*$^{+/+}$) CFs after ISO treatment. Upper panel: * P=2.4x10^{-7}, ** P=4.7x10^{-11}, † P=1.2x10^{-7}, Veh. vs. ISO; # P=8.9x10^{-5}, ## P=1.8x10^{-6}, ‡ P=1.7x10^{-8}, ISO vs. ISO, Halo. Lower panel: * P=3.9x10^{-5}, ** P=1.9x10^{-8}, † P=1.4x10^{-6}, *Eprs*$^{+/+}$ Veh. vs. *Eprs*$^{+/+}$ ISO; # P=0.15, ## P=0.0029, ‡ P=0.095, *Eprs*$^{+/+}$ ISO vs. *Eprs*$^{+/-}$ ISO. Comparisons were performed by non-parametric Kruskal-Wallis test with Conover-Iman method for post hoc pairwise comparisons and Benjamini-Hochberg correction.

(A) EPRS overexpression induces COL3A1 protein expression indicated by IF. EPRS-overexpressing and control lentiviruses were used to infect primary mouse CFs with or without TGF-β (10 ng/ml) treatment. Scale bar: 100 μM. n>120 cells for COL3A1 protein expression measurement from 3 biologically replicated experiments.

Comparisons were performed by non-parametric unpaired Mann-Whitney test for C, E and non-parametric Kruskal-Wallis test with Conover-Iman method for post hoc pairwise comparisons and Benjamini-Hochberg correction for G.

Online Figure VI. EPRS regulates Pro-rich protein expression in fibroblasts.

(A) Differentially expressed genes identified by RNA-Seq and polysome-Seq are indicated by dot plot. Translation efficiency (TE) is indicated by the ratio between light polysome and polysome-free fraction. The colored dots indicate statistically significantly changed genes in either RNA-Seq or polysome-Seq. The genes with P_{adj}<0.05 in either of three different groups (ratio of Halo vs. Veh. treated samples for total RNA, non-polysome, and light polysome) were considered as significantly changed genes. All significantly changed genes were divided into four areas based on log_2FC of total mRNAs and light polysome mRNAs.

(B) A majority of genes show a synergistic change at mRNA and translational levels after EPRS inhibition by Halo. The number of genes is shown with changes at both translation efficiency (the ratio of heavy or light polysome to polysome-free fraction) and steady-state mRNA levels in all four areas.

(C) Log_2FC of translation efficiency and steady-state mRNA level for all the collagens (typical Pro-rich genes as a positive control gene panel for Area 1).

(D) Log_2FC of translation efficiency and steady-state mRNA level for all cytosolic aminoacyl-tRNA synthetase (amino acid starvation response markers as a positive control gene panel for Area 3).

Online Figure VII. Halo downregulated collagen protein translation.

(A-B) Genetic codon composition in mouse *Col1a1* and *Col3a1* genes and global mouse genome (https://www.genscript.com/tools/codon-frequency-table).

(C-D) Halo reduced polysome association of collagen mRNAs in primary mouse CFs. **C**. * P=1.8x10^{-5}, ** P=4.6x10^{-6}, # P=7.7x10^{-5}, Halo vs. Veh. **D**. * P=1.2x10^{-4}, ** P=1.2x10^{-4}, # P=1.2x10^{-4}, Halo vs. Veh. Comparisons were performed by non-parametric Kruskal-Wallis test with Conover-Iman method for post hoc pairwise comparisons and Benjamini-Hochberg correction.

(E) Translationally dysregulated genes are indicated by overlapping changed genes in the same area of heavy polysome **(Figure 4B)** and light polysome **(Online Figure VIA)**. Genes decreased at the translational level and increased at steady-state mRNA level (Area 2) or increased at the translational level and decreased at steady-state mRNA level (Area 4) at translation and steady-state mRNA levels are shown.

(F) KEGG pathway analyses of the gene cluster in Area 4 from **(E)**. DAVID Bioinformatics Resources 6.8 was used.

Online Figure VIII. LTBP2 is a novel downstream target of EPRS.

(A) Dot plot of mass spectrometry data of human CFs treated with 300 nM Halo (experiments performed by Glaxo Smith Kline)[15].

(B) *Ltbp2* mRNA levels are reduced by Halo in both RNA-Seq and polysome-Seq of Halo-treated NIH/3T3 mouse fibroblasts.

(C) Polysome-associated *Ltbp2* mRNA levels are reduced by Halo in primary mouse CFs. ns: P=0.060, * P=0.014, # P=0.027, Halo vs. Veh. by non-parametric Kruskal-Wallis test with Conover-Iman method for post hoc pairwise comparisons and Benjamini-Hochberg correction.

(D) EPRS inhibition reverses ISO-induced polysome association of *Ltbp2* mRNA in primary mouse CFs. ns: P=0.60, ** P=1.0x10^{-6}, † P=3.1x10^{-6}, Veh. vs. ISO; # P=2.5x10^{-6}, ## P=1.5x10^{-5}, ‡ P=5.6x10^{-5} ISO vs. ISO, Halo. by non-parametric Kruskal-Wallis test with

Conover-Iman method for post hoc pairwise comparisons and Benjamini-Hochberg correction.

(E) Polysome-associated *Ltbp2* mRNA is reduced in primary *Eprs*$^{+/-}$ CFs compared to WT (*Eprs*$^{+/+}$) CFs after ISO treatment. * P=2.5x10^{-5}, ** P=0.036, † P=1.4x10^{-6}, *Eprs*$^{+/+}$, Veh. vs. *Eprs*$^{+/+}$, ISO; # P=1.9x10^{-10}, ## P=5.6x10^{-8}, ‡ P=5.1x10^{-9} *Eprs*$^{+/+}$, ISO vs. *Eprs*$^{+/-}$, ISO by non-parametric Kruskal-Wallis test with Conover-Iman method for post hoc pairwise comparisons and Benjamini-Hochberg correction.

Online Figure IX. SULF1 is a human and mouse cardiac fibrosis marker.

(A) RT-qPCR measurement of *Sulf1* mRNA expression in isolated primary mouse CFs and CMs. *Postn* and *Myh6* mRNA expression was measured as indication of quality control of CM and CF isolation.

(B) *SULF1* mRNA expression is increased in dilated cardiomyopathy (DCM, n=82) and ischemic heart failure (IHF, n=95) patients compared to non-failing (NF, n=80) donor heart tissues from a publicly available microarray dataset GSE57345[41].

(C-D) SULF1 expression is correlated with COL1A1 **(C)** and COL3A1 **(D)** in the validation cohort of human subjects. Pearson correlation coefficient was presented.

(E) Immunostaining shows SULF1 is highly expressed in α-SMA positive myofibroblasts in failing human hearts. Scale bar: 20 μm.

(F-G) Quantification of α-SMA **(F)** and SULF1 **(G)** protein expression in failing human and non-failing hearts in immunofluorescence staining in **(E)**. n>200 cells from three heart tissue samples were analyzed.

(H-I) Immunostaining shows SULF1 is highly expressed in α-SMA positive myofibroblasts in a TAC-induced mouse HF model **(H)** and quantification of SULF1 intensity in **(I)**. Scale bar: 20 μm. n>150 cells from three mouse heart samples were analyzed.

Comparisons were performed by non-parametric unpaired Mann-Whitney test for A, I, and non-parametric Kruskal-Wallis test with Conover-Iman method for post hoc pairwise comparisons and Benjamini-Hochberg correction for B, F, G.

Online Figure X. The effect of SULF1 knockdown and overexpression on TGF-β-activated myofibroblast formation.

(A-B) IF staining shows reduced protein expression of COL1A1 and α-SMA by siRNA-mediated knockdown of Sulf1 in TGF-β-treated primary mouse CFs. Scale bar: 40 μm.

(C-D) SULF1 overexpression induces COL1A1 and α-SMA protein expression indicated by IF. Lentiviral Sulf1 and control lentivirus were used to infect primary mouse CFs with or without TGF-β (10 ng/ml) treatment. Scale bar: 100 μM. n>200 cells from 3 biologically replicated experiments.

Online Figure XI. Knockdown of CysRS or inhibition of LeuRS does not reduce COL1A1 protein expression.

(A) siRNA-mediated knockdown of CysRS does not significantly reduce COL1A1 protein expression in NIH/3T3 fibroblast cells.

(B) LeuRS inhibitor leucinol does not reduce COL1A1 protein expression when used to treat NIH/3T3 fibroblast cells at 10-2000 nM.

Online Figure XII. Effect of genetic knockdown or Halo inhibition of EPRS on POSTN protein expression.

(A) POSTN protein expression is slightly but significantly reduced in *Eprs* insufficient primary CFs isolated from *Eprs*$^{+/-}$ mice. Quantification is performed for n>220 cells from 3 biologically replicated experiments. Scale bar: 100 μm.

(B-C) POSTN protein expression is markedly reduced in Halo-treated primary CFs isolated from *Eprs*$^{+/-}$ mice. Both IF **(B)** and IB **(C)** were performed (n=3). In **(B)**, quantification is performed for n>150 cells from 3 biologically replicated experiments. Scale bar: 100 μm.

Comparisons were performed by non-parametric Kruskal-Wallis test with Conover-Iman method for post hoc pairwise comparisons and Benjamini-Hochberg correction for A-C.

A

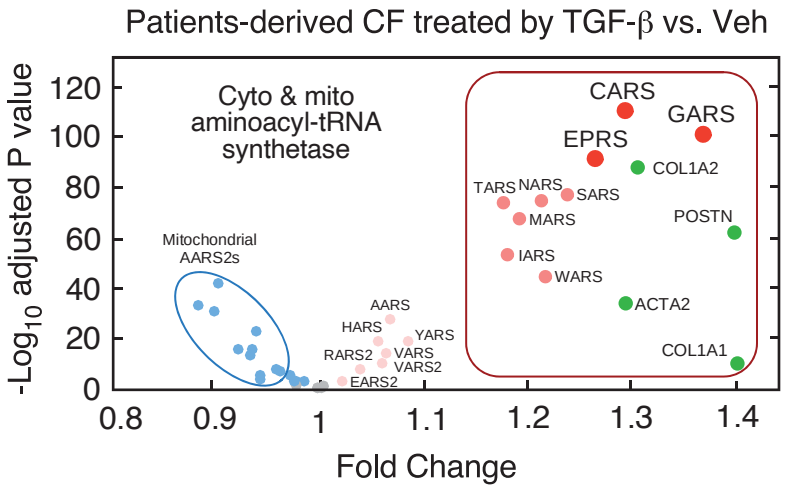

B

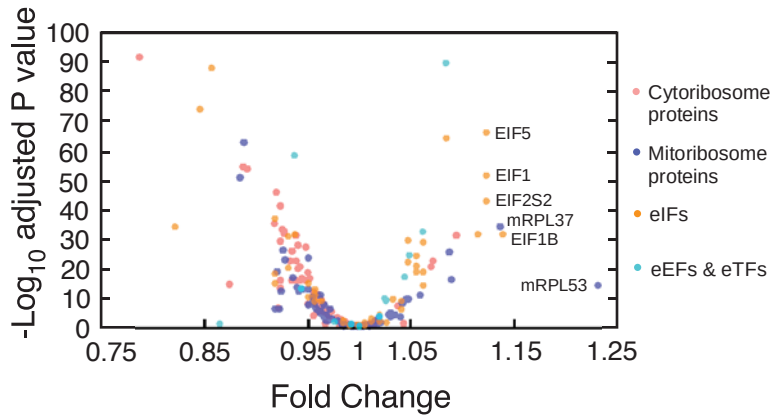

Online Figure I

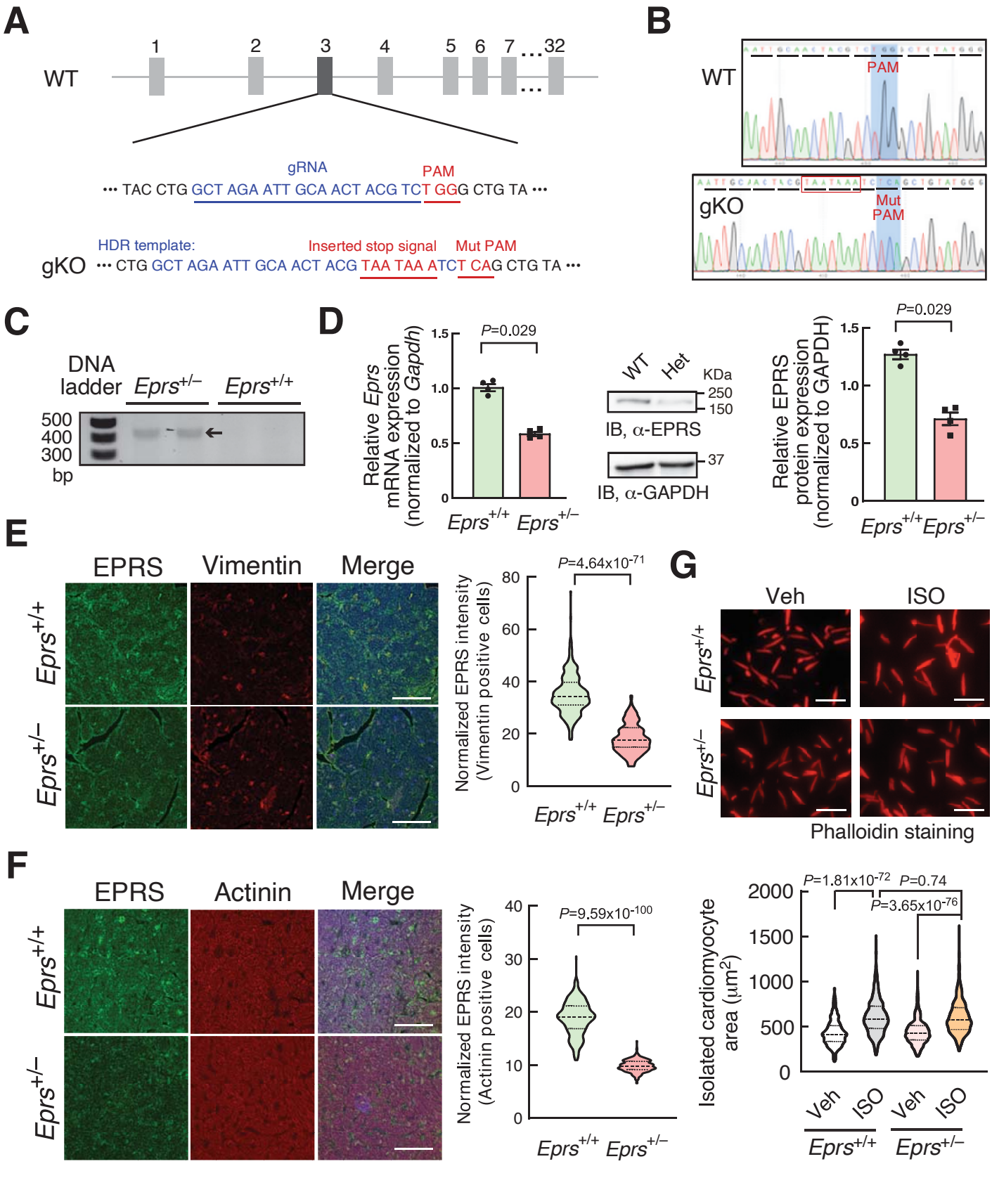

Online Figure II

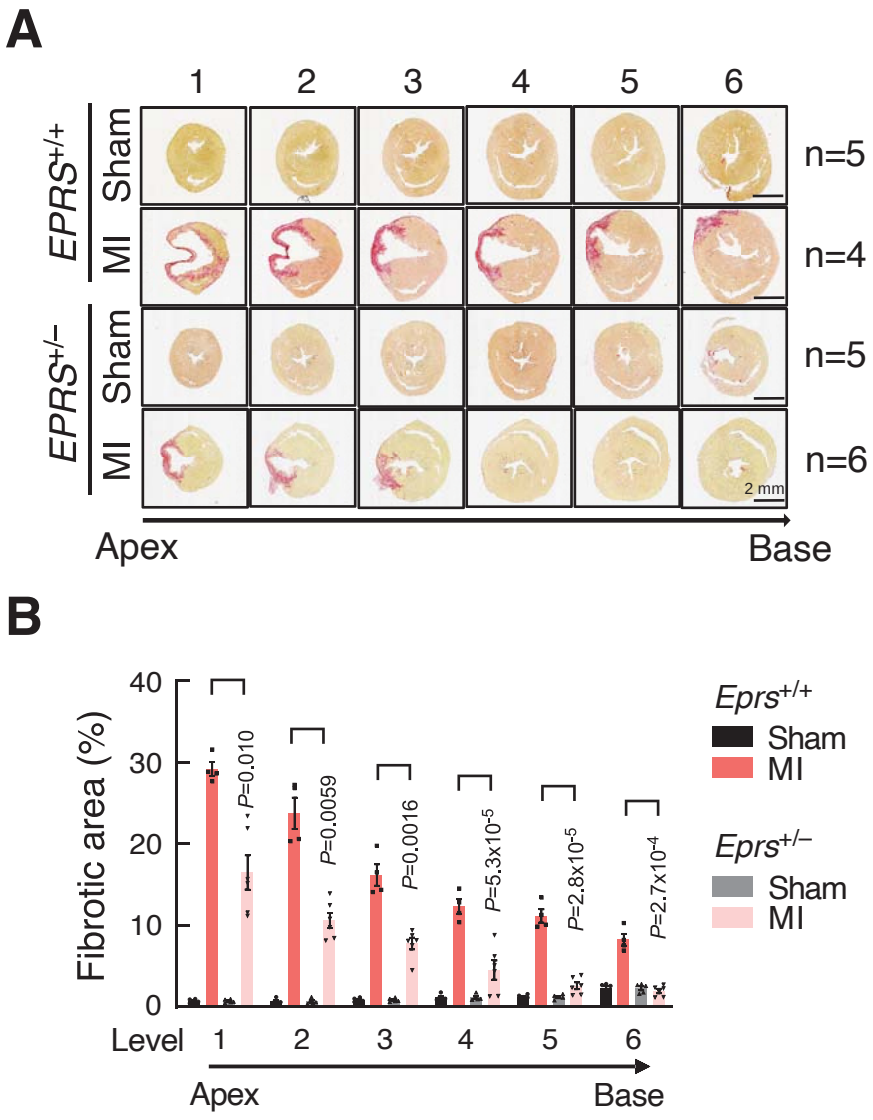

Online Figure III

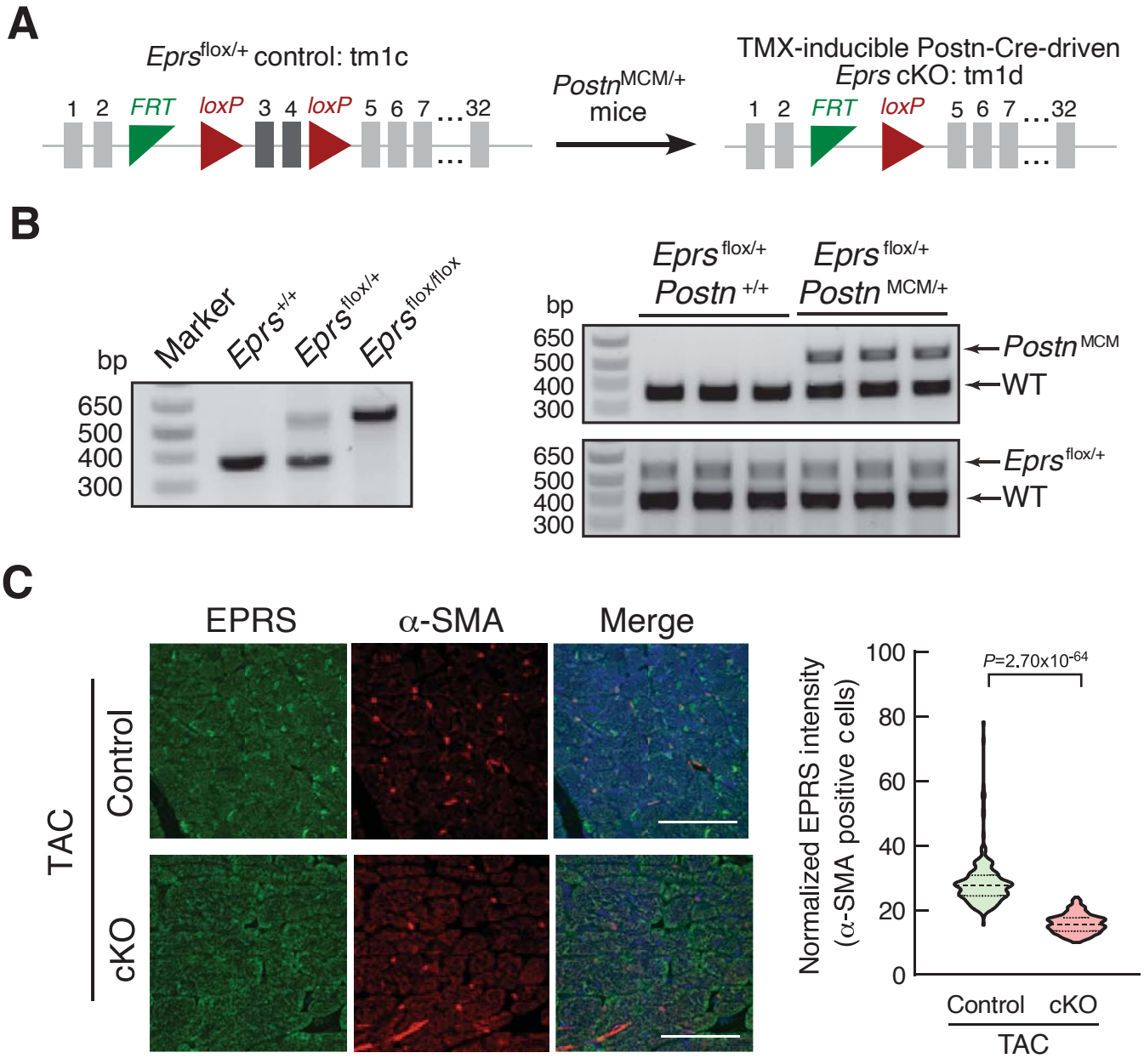

Online Figure IV

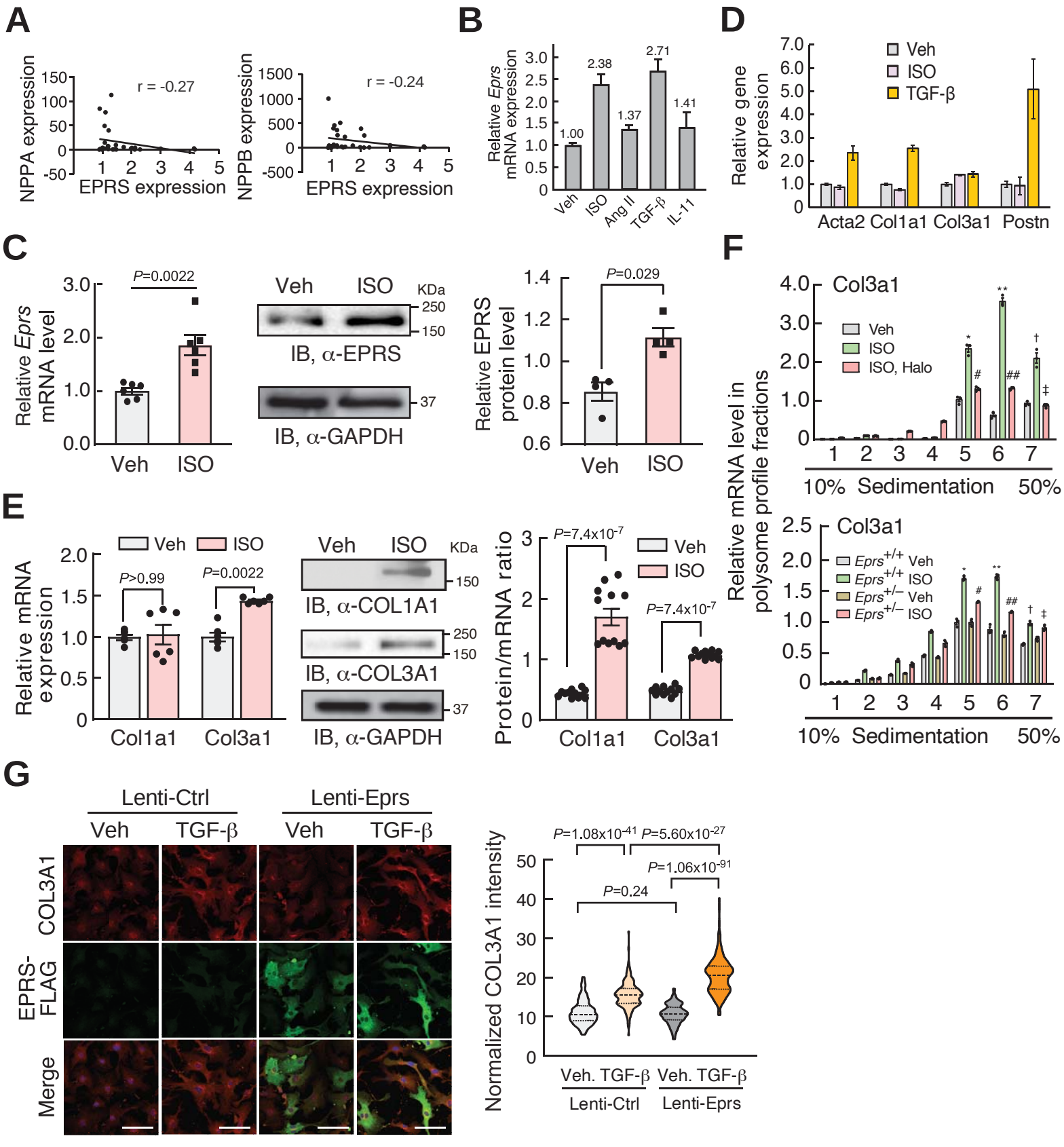

Online Figure V

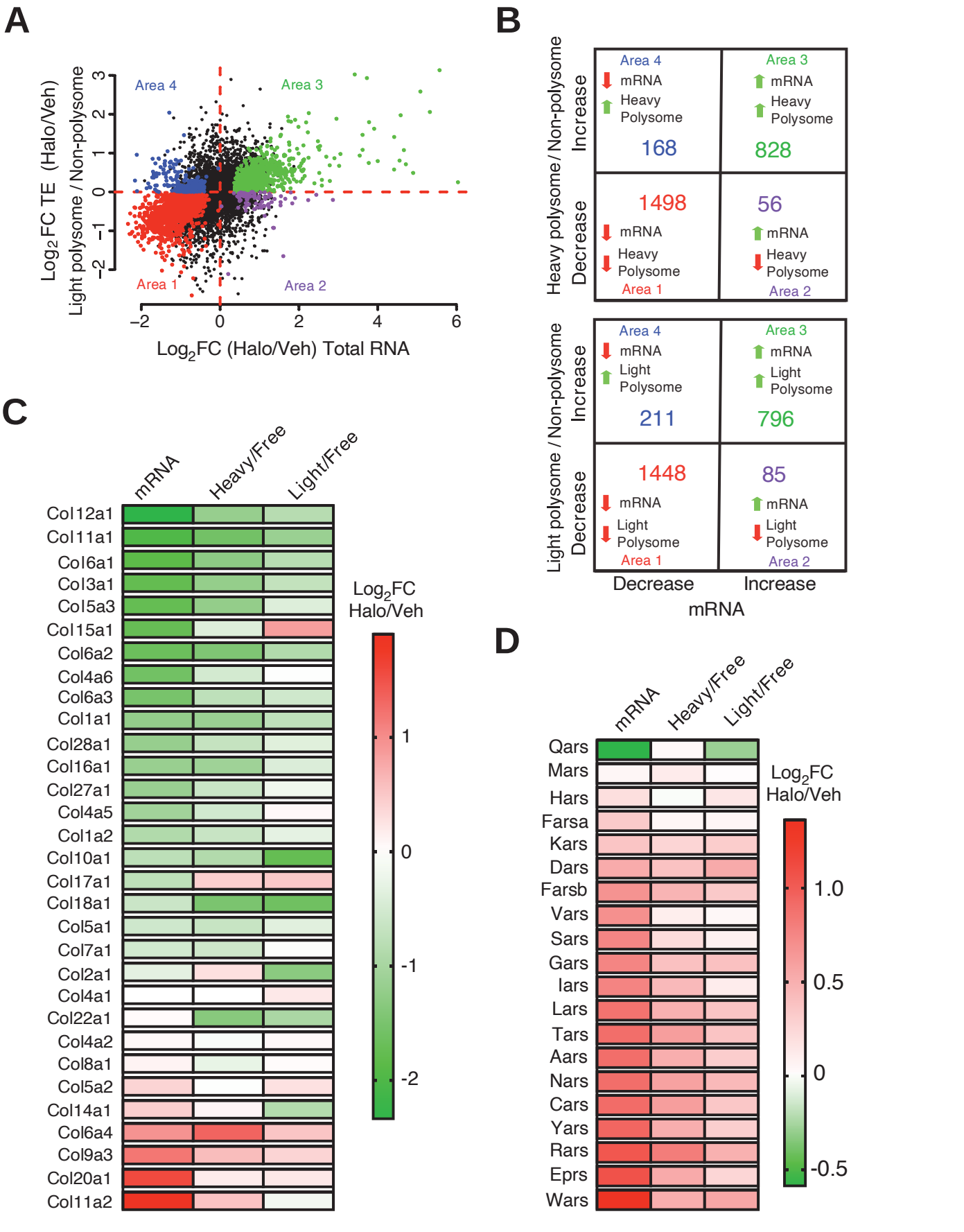

Online Figure VI

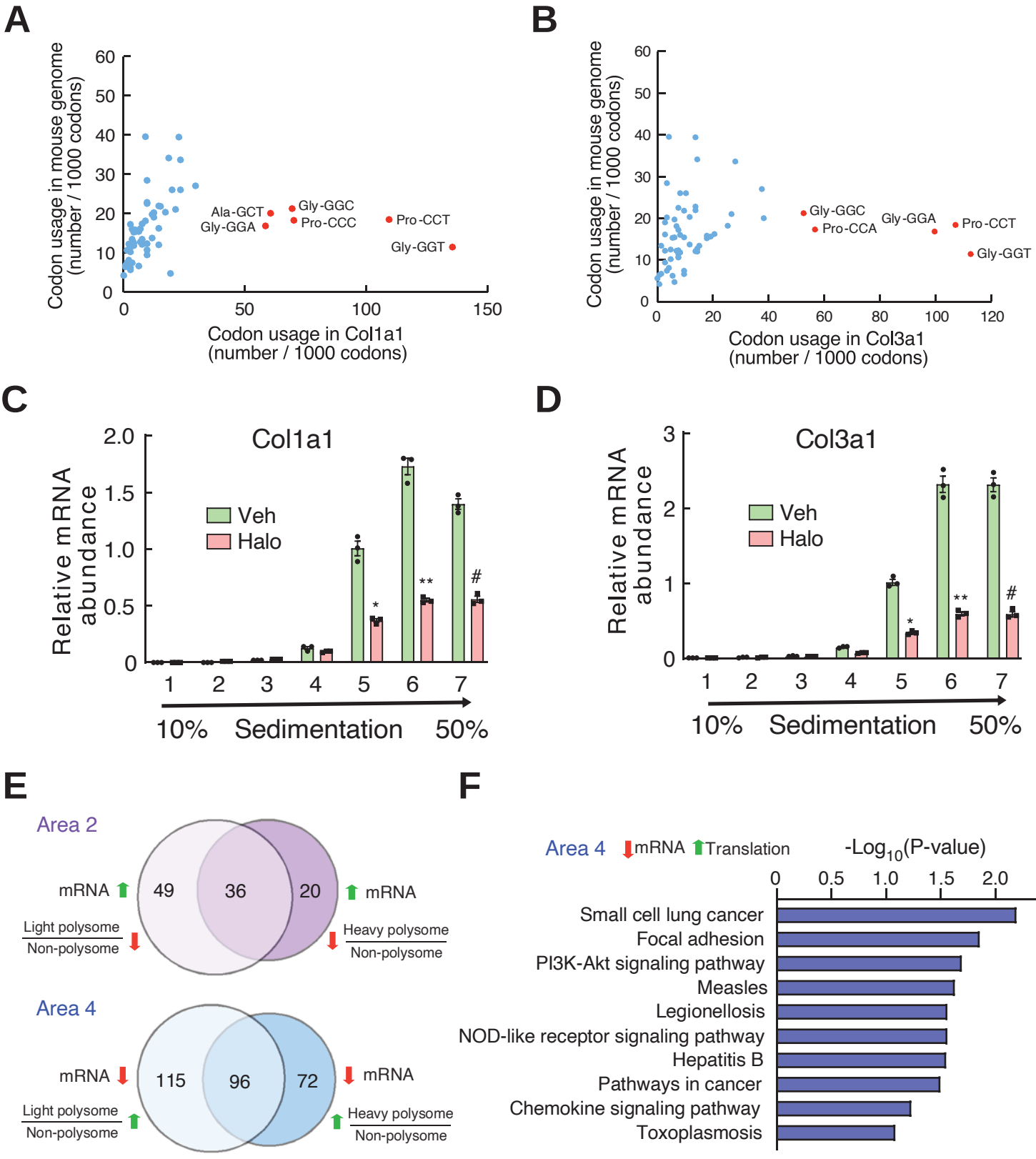

Online Figure VII

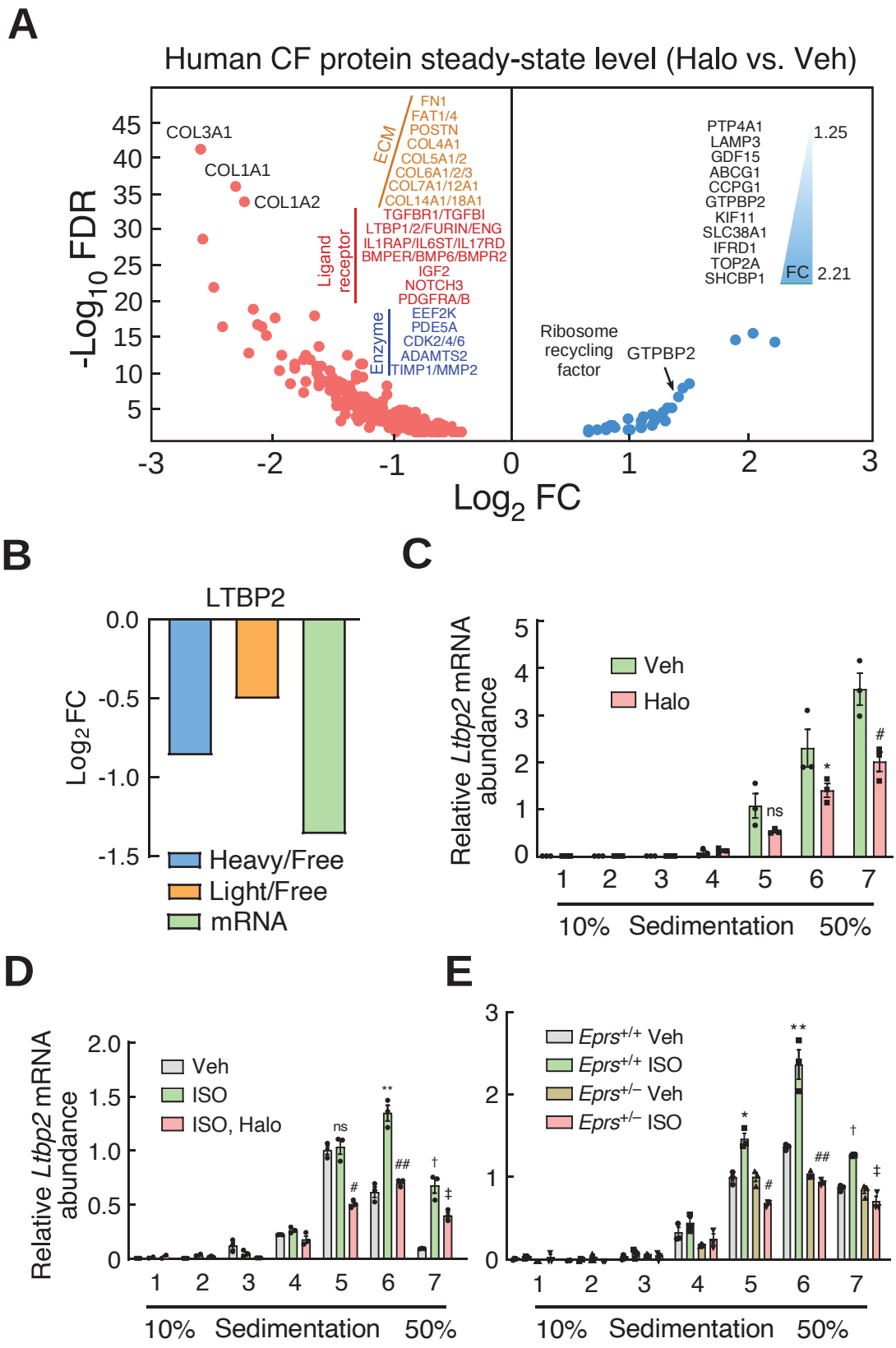

Online Figure VIII

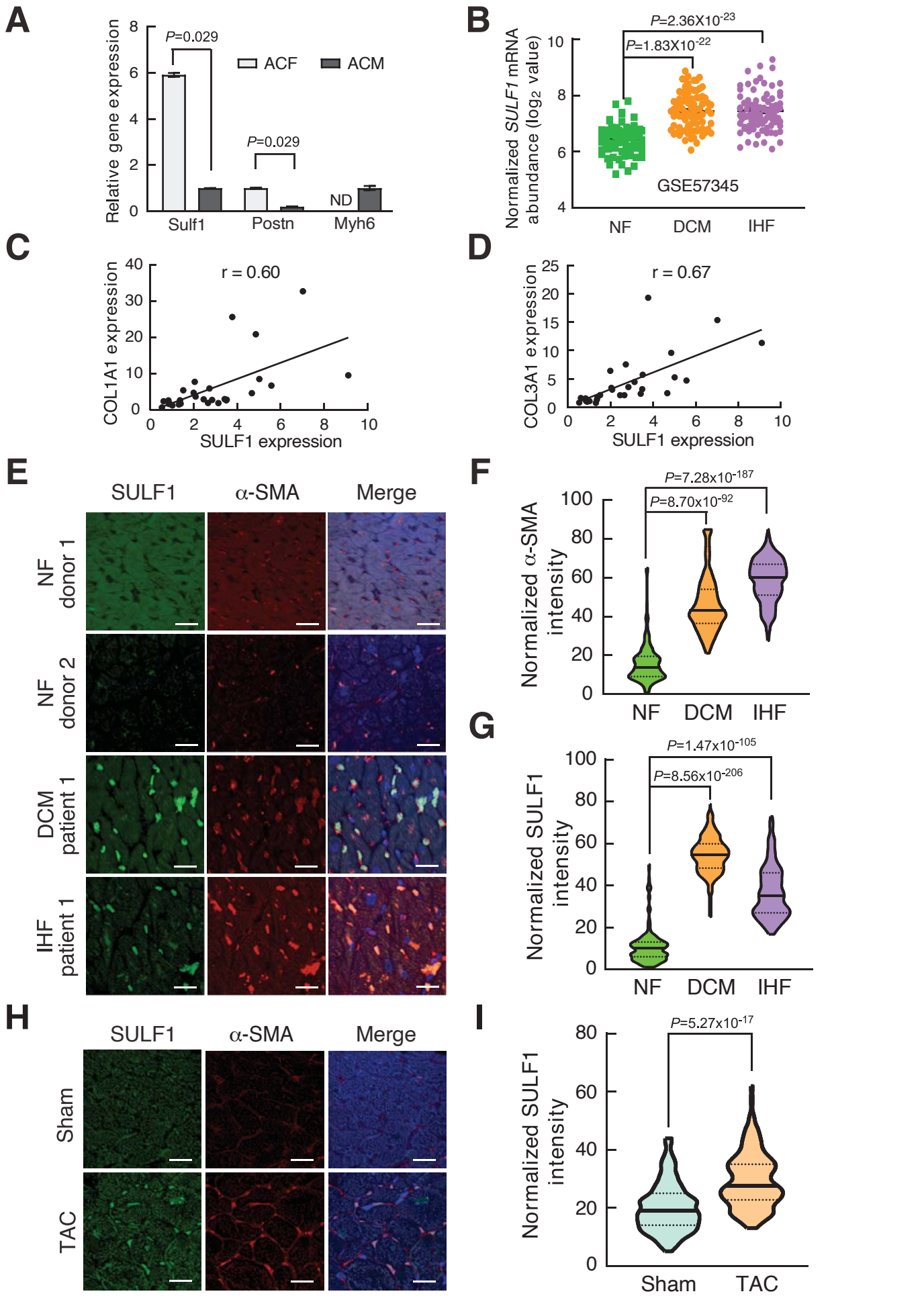

Online Figure IX

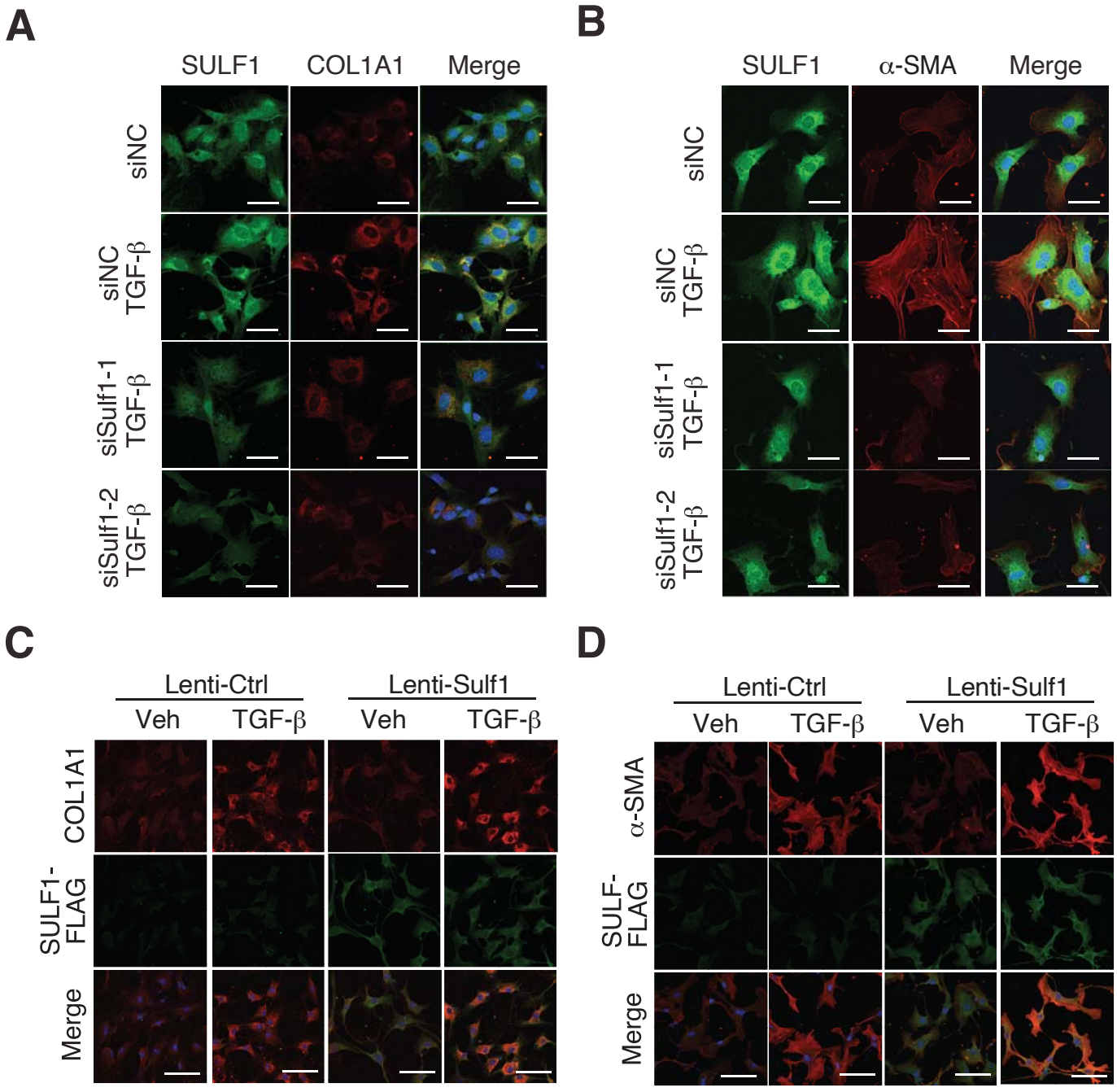

Online Figure X

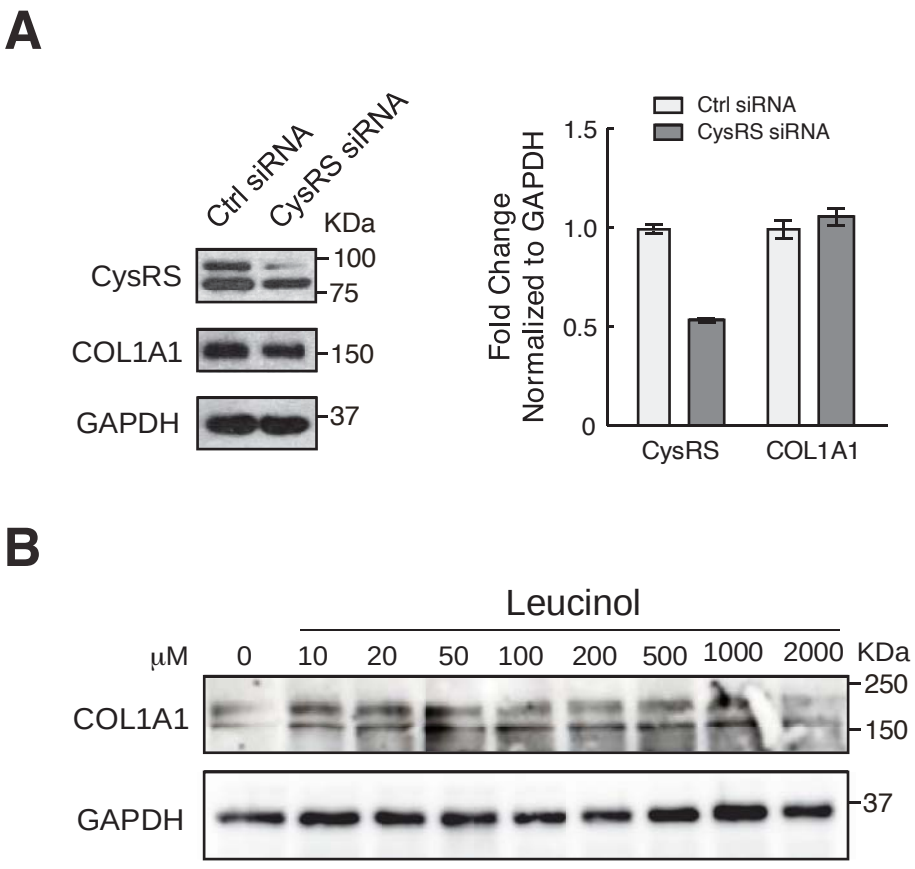

Online Figure XI

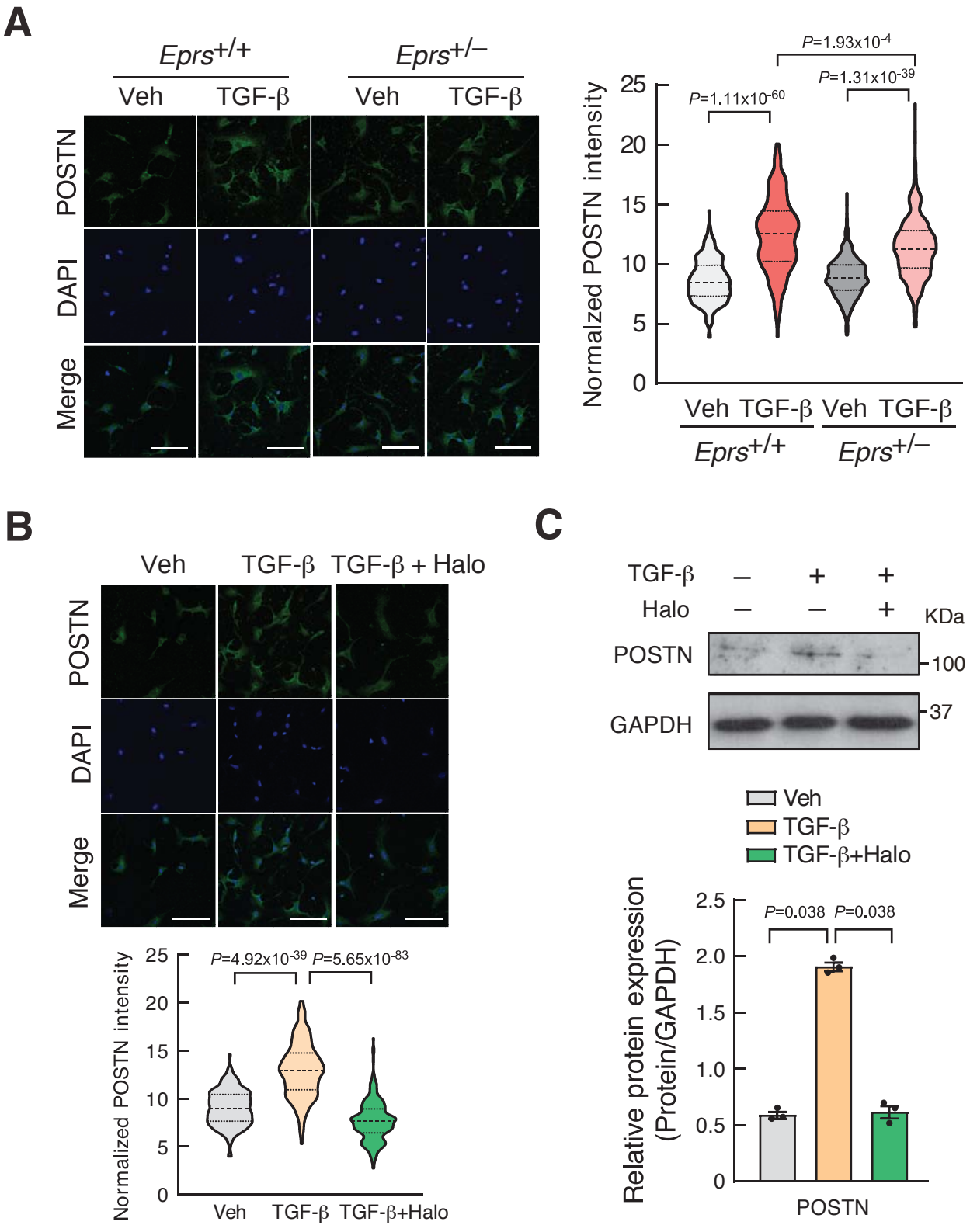

Online Figure XII

Online Table Legends

Online Table I: Reanalysis of mRNA expression of all the translation machinery component genes in TGF-β- versus vehicle-treated human cardiac fibroblasts from published database (*Nature* 2017 552(7683): 110-115).

Online Table II: Summary of echocardiograph data in *Eprs*$^{+/+}$ and *Eprs*$^{+/-}$ mice after 8 weeks of Sham or TAC surgeries using the preventive model.

Online Table III: Summary of echocardiograph data in control and *Eprs* cKO mice after 8 weeks of Sham or TAC surgeries using the reversal model.

Online Table IV: Log_2FC of mRNAs in RNA-Seq and 3 different pooled fractions of polysome-Seq upon halofuginone treatment. RNA-Seq and polysome-Seq were performed in 100 nM Halo or Veh. treated fibroblast cells. The log_2FC and P_{adj} value were calculated for all the mRNAs between Halo and Veh. in all four groups (total RNA, non polysome, light polysome, and heavy polysome).

Online Table V: Differentially expressed genes in four areas of gene clusters. The genes with $p \leq 0.05$ in either of four different groups (ratio of Halo vs. Veh. treated samples for total RNA, ribosome free, light polysome, and heavy polysome) were considered as significantly changed genes. All significantly changed genes were divided into four areas based on log_2FC of total mRNAs and polysome mRNAs (heavy or light polysome). Area 1: total mRNA decreased and polysomal mRNA decreased; Area 2: total mRNA increased and polysomal mRNA decreased; Area 3: total mRNA increased and polysomal mRNA increased; Area 4: total mRNA decreased and polysomal mRNA increased.

Online Table VI: KEGG pathway analyses in four different areas of gene clusters. All the genes in four areas were subjected to KEGG pathway analyses in DAVID Bioinformatics Resources and the significantly enriched genes were listed. Note: No KEGG pathways was significantly enriched in Area 4 due to a limited number of genes in this area.

Online Table VII: Proline motifs analyses in Area 1 and 3. The number of proline motifs were quantified in the genes of Area 1 and 3.

Online Table VIII: The list of PP motif containing genes that were quantified across human and mouse proteomes.

Online Table IX: The list of genes containing PP motifs and undergoing downregulation at polysomal mRNA and steady state protein levels. Based on the gene list in Online Table VIII, the

genes containing PP motif in both human and mouse were defined as conserved PP motif containing genes (first sub-table). By overlapping of human/mouse conserved PP motif containing genes (first sub-table), Halo-triggered polysomal mRNA-downregulated genes (second sub-table), and mass spectrometry-detected protein-decreased genes (third sub-table), 83 common hits (fourth sub-table) were found significantly downregulated by low dose of Halo at the translational level.

Online Table X: Gene ontology (GO) analysis of the overlapped 83 genes. GO analysis was performed for the 83 overlapped genes and fold change of all genes in top 5 GO_BP terms were listed.

Online Table XI: SYBR Green primers and Taqman probes used for RT-qPCR in this research.

Online Table XII: Overall *P* values of non-parametric tests for comparing N≥3 groups of samples.

Online Table II: Summary of echocardiograph data in *Eprs*$^{+/+}$ and *Eprs*$^{+/-}$ mice after 8 weeks of Sham or TAC surgeries using the preventive model (related to Figure 2H).

	Eprs$^{+/+}$ Sham (N=14)		*Eprs*$^{+/+}$ TAC (N=6)		*Eprs*$^{+/-}$ Sham (N=11)		*Eprs*$^{+/-}$ TAC (N=7)	
Parameters	**Baseline**	**8 wk post-surgery**	**Baseline**	**8 wk post-surgery**	**Baseline**	**8 wk post-surgery**	**Baseline**	**8 wk post-surgery**
Heart Rate (BPM)	568.55±5.31	605.13±6.52	569.17±11.6	595.25±19.09	575.35±7.07	613.06±9.95	549.32±8.64	577.16±8.7
LVV, s (μL)	8.43±0.35	11.3±0.71	11.77±2.29	**25.32±3.61*****	11.81±1.35	12.06±0.96	12.75±2.5	**13.71±1.38**$^{\#}$
LVV, d (μL)	42.85±1.74	52.72±1.88	44.27±2.58	60.49±5.88	47.47±2.52	50.29±2.47	40.47±3.38	**43.58±2.91**$^{\#}$
Stroke Volume (μL)	34.41±1.41	41.42±1.26	32.5±1.83	**35.17±2.55***	35.66±1.44	38.22±1.56	27.72±1.7	29.87±1.99
EF (%)	80.32±0.28	78.78±0.68	74.02±4.1	**59.02±2.39*****	75.72±1.6	76.37±0.88	69.68±4.12	**68.8±1.99**$^{\#\#}$
FS (%)	47.79±0.29	46.59±0.63	42.58±3.39	**30.83±1.57*****	43.73±1.41	44.25±0.79	38.86±3.3	**37.7±1.6**$^{\#\#}$
Cardiac Output (mL/min)	19.58±0.85	25.08±0.84	18.55±1.25	**20.73±0.96****	20.46±0.72	23.39±0.96	15.24±0.98	17.29±1.32
LVM (mg)	58.55±2.89	74.15±2.18	62.77±2.37	**116.08±5.13*****	70.03±3.64	69.83±3.5	64.12±4.82	93.07±6.19
LVID, s (mm)	1.69±0.04	1.9±0.04	1.69±0.07	**2.41±0.12****	1.79±0.1	1.94±0.08	1.65±0.08	**1.88±0.06**$^{\#}$
LVID, d (mm)	3.22±0.06	3.54±0.04	3.17±0.08	3.54±0.11	3.28±0.07	3.44±0.08	3.04±0.02	**3.13±0.07**$^{\#}$
LVAWD, s (mm)	1.08±0.03	1.16±0.02	1.04±0.08	1.19±0.09	1.03±0.05	1.01±0.05	0.98±0.08	1.23±0.06
LVAWD, d (mm)	0.69±0.02	0.73±0.01	0.74±0.04	**0.95±0.06****	0.73±0.03	0.7±0.02	0.74±0.03	0.89±0.03
LVPWD, s (mm)	0.9±0.02	0.9±0.01	0.86±0.02	**1.03±0.03****	0.87±0.03	0.88±0.03	0.84±0.05	1.04±0.05
LVPWD, d (mm)	0.56±0.01	0.56±0.01	0.55±0.02	**0.82±0.04*****	0.65±0.03	0.6±0.03	0.62±0.03	0.86±0.05

BPM: Beats per minute. LVV, d/s: left ventricular volume, diastole/systole. EF: ejection fraction. FS: fractional shortening. LVM: left ventricular mass. LVAWD, d/s: left ventricular anterior wall diameter, diastole/systole. LVID, d/s: left ventricular internal diameter, diastole/systole. LVPWD, d/s: left ventricular posterior wall diameter, diastole/systole. Values are presented as mean ± SEM. *P* values were calculated by non-parametric Kruskal-Wallis test with Conover-Iman method for post hoc comparisons and Benjamini-Hochberg method for type I error correction. All comparisons were made for 8-week post TAC. * $P<0.05$, ** $P<0.01$, *** $P<0.001$ for *Eprs*$^{+/+}$ (WT) TAC vs. *Eprs*$^{+/+}$ Sham; $^{\#}$ $P<0.05$, $^{\#\#}$ $P<0.01$ for *Eprs*$^{+/-}$ (Het KO) TAC vs. *Eprs*$^{+/+}$ TAC.

LVV, s: WT TAC vs. WT Sham $P=3.32\times10^{-4}$; Het KO TAC vs. WT TAC $P=0.022$; Het KO TAC vs. Het KO Sham $P=0.42$.

LVV, d: WT TAC vs. WT Sham $P=0.42$; Het KO TAC vs. WT TAC $P=0.039$; Het KO TAC vs. Het KO Sham $P=0.17$.

Stroke Volume: WT TAC vs. WT Sham $P=0.018$; Het KO TAC vs. WT TAC $P=0.18$; Het KO TAC vs. Het KO Sham $P=0.012$.

EF: WT TAC vs. WT Sham $P=3.3\times10^{-8}$; Het KO TAC vs. WT TAC $P=0.002$; Het KO TAC vs. Het KO Sham $P=0.072$.

FS: WT TAC vs. WT Sham $P=3.3\times10^{-8}$; Het KO TAC vs. WT TAC $P=0.002$; Het KO TAC vs. Het KO Sham $P=0.072$.

Cardiac Output: WT TAC vs. WT Sham $P=0.0084$; Het KO TAC vs. WT TAC $P=0.16$; Het KO TAC vs. Het KO Sham $P=0.0045$.

LV Mass: WT TAC vs. WT Sham P=6.29x10^{-5}; Het KO TAC vs. WT TAC P=0.060; Het KO TAC vs. Het KO Sham P=6.98x10^{-4}.
LVID, s: WT TAC vs. WT Sham P=0.0094; Het KO TAC vs. WT TAC P=0.015; Het KO TAC vs. Het KO Sham P=0.70.
LVID, d: WT TAC vs. WT Sham P=0.65; Het KO TAC vs. WT TAC P=0.046; Het KO TAC vs. Het KO Sham P=0.049.
LVAWD, s: WT TAC vs. WT Sham P=0.53; Het KO TAC vs. WT TAC P=0.87; Het KO TAC vs. Het KO Sham P=0.066.
LVAWD, d: WT TAC vs. WT Sham P=0.0012; Het KO TAC vs. WT TAC P=0.94; Het KO TAC vs. Het KO Sham P=4.56x10^{-5}.
LVPWD, s: WT TAC vs. WT Sham P=0.0073; Het KO TAC vs. WT TAC P=0.71; Het KO TAC vs. Het KO Sham P=0.0025.
LVPWD, d: WT TAC vs. WT Sham P=1.95x10^{-5}; Het KO TAC vs. WT TAC P=0.64; Het KO TAC vs. Het KO Sham P=3.83x10^{-5}.

Online Table III: Summary of echocardiograph data in control and *Eprs* cKO mice after 8 weeks of Sham or TAC surgeries using the reversal model (related to Figure 3I).

Parameters (8 wk post-surgery)	Control Sham (N=3)	Control TAC (N=5)	*Eprs* cKO Sham (N=4)	*Eprs* cKO TAC (N=6)
Heart Rate (BPM)	586.06 ± 5.13	490.72 ± 5.70	530.92 ± 18.42	523.13 ± 8.89
LVV, s (μL)	13.16 ± 1.27	**39.15 ± 7.66***	12.60 ± 2.16	21.84 ± 6.10
LVV, d (μL)	58.56 ± 1.08	78.33 ± 9.98	52.10 ± 5.23	61.29 ± 7.24
Stroke Volume (μL)	45.42 ± 0.20	39.18 ± 4.55	39.49 ± 3.09	39.45 ± 1.81
EF (%)	77.57 ± 1.72	**51.56 ± 5.08****	76.41 ± 1.96	**66.80 ± 4.54**†
FS (%)	45.56 ± 1.61	**26.42 ± 3.16****	44.36 ± 1.74	**36.92 ± 3.20**†
Cardiac Output (mL/min)	26.61 ± 0.35	19.30 ± 2.43	20.91 ± 1.55	20.64 ± 1.01
LVM (mg)	66.41 ± 2.45	**122.48 ± 11.94****	69.79 ± 1.83	**110.55 ± 11.13**##
LVID, s (mm)	2.02 ± 0.08	**3.08 ± 0.27***	1.97 ± 0.14	2.39 ± 0.24
LVID, d (mm)	3.71 ± 0.03	**4.16 ± 0.23***	3.52 ± 0.15	3.76 ± 0.17
LVAWD, s (mm)	1.06 ± 0.04	1.15 ± 0.065	1.09 ± 0.03	1.24 ± 0.02
LVAWD, d (mm)	0.62 ± 0.02	**0.85 ± 0.068***	0.71 ± 0.03	0.87 ± 0.04
LVPWD, s (mm)	0.93 ± 0.03	0.92 ± 0.089	0.90 ± 0.07	1.04 ± 0.05
LVPWD, d (mm)	0.52 ± 0.02	**0.72 ± 0.075***	0.57 ± 0.07	**0.77 ± 0.05#**

BPM: Beats per minute. LVV, d/s: left ventricular volume, diastole/systole. EF: ejection fraction. FS: fractional shortening. LVM: left ventricular mass. LVAWD, d/s: left ventricular anterior wall diameter, diastole/systole. LVID, d/s: left ventricular internal diameter, diastole/systole. LVPWD, d/s: left ventricular posterior wall diameter, diastole/systole. Values are presented as mean ± SEM. *P* values were calculated by non-parametric Kruskal-Wallis test with Conover-Iman method for post hoc comparisons and Benjamini-Hochberg method for type I error correction. * P<0.05, ** P<0.01 for Control Sham vs Control TAC; # P<0.05, ## P<0.01 for *Eprs* cKO Sham vs cKO TAC; † P<0.05 for *Eprs* cKO TAC vs Control TAC.

LVV, s: Control TAC vs. Control Sham *P*=0.019; cKO TAC vs. Control TAC *P*=0.16; cKO TAC vs. cKO Sham *P*=0.16.
LVV, d: Control TAC vs. Control Sham *P*=0.52; cKO TAC vs. Control TAC *P*=0.34; cKO TAC vs. cKO Sham *P*=0.54.
Stroke Volume: Control TAC vs. Control Sham *P*=0.30; cKO TAC vs. Control TAC *P*=0.88; cKO TAC vs. cKO Sham *P*=0.92.
Cardiac Output: Control TAC vs. Control Sham *P*=0.099; cKO TAC vs. Control TAC *P*=0.55; cKO TAC vs. cKO Sham *P*>0.99.
EF: Control TAC vs. Control Sham *P*=0.0022; cKO TAC vs. Control TAC *P*=0.047; cKO TAC vs. cKO Sham *P*=0.054
FS: Control TAC vs. Control Sham *P*=0.0016; cKO TAC vs. Control TAC *P*=0.039; cKO TAC vs. cKO Sham *P*=0.039.
LV Mass: Control TAC vs. Control Sham *P*=0.0017; cKO TAC vs. Control TAC P=0.63; cKO TAC vs. cKO Sham *P*=0.0019.
LVID, s: Control TAC vs. Control Sham *P*=0.021; cKO TAC vs. Control TAC *P*=0.15; cKO TAC vs. cKO Sham *P*=0.15.
LVID, d: Control TAC vs. Control Sham *P*=0.021; cKO TAC vs. Control TAC *P*=0.15; cKO TAC vs. cKO Sham *P*=0.15.

LVAWD, s: Control TAC vs. Control Sham *P*=0.33; cKO TAC vs. Control TAC *P*=0.18; cKO TAC vs. cKO Sham *P*=0.051.
LVAWD, d: Control TAC vs. Control Sham *P*=0.018; cKO TAC vs. Control TAC *P*=0.67; cKO TAC vs. cKO Sham *P*=0.10.
LVPWD, s: Control TAC vs. Control Sham *P*=0.76; cKO TAC vs. Control TAC *P*=0.73; cKO TAC vs. cKO Sham *P*=0.73.
LVPWD, d: Control TAC vs. Control Sham *P*=0.040; cKO TAC vs. Control TAC *P*=0.58; cKO TAC vs. cKO Sham *P*=0.040.

Online Table XI: SYBR Green primers and Taqman probes used for RT-qPCR in this research.

SYBR Green RT-qPCR primers		
Gene	**Forward Primer (5'-3')**	**Reverse Primer (5'-3')**
hGAPDH	GGAGCGAGATCCCTCCAAAAT	GGCTGTTGTCATACTTCTCATGG
hEPRS	GAAATGCCAACATCAGGGTCA	AGCCACTCTATTGTAAAGGACCA
hNPPA	TCCCATGTACAATGCCGTGTCC	CCCGCTTCTTCATTCGGCTCA
hNPPB	GCTCCTGCTCTTCTTGCATC	CTCCAGGGATGTCTGCTCCA
hSULF1	GCACGAGTTCTAACAATAACACC	GCTGATTCAAAATGCCTCGTTC
RLuc	AACATTATCATGGCCTCGT	CACCTTCAACAATAGCATT
mGapdh	AGGTCGGTGTGAACGGATTTG	TGTAGACCATGTAGTTGAGGTCA
mEprs	CCGTCTGTGTCACTTATGAGC	GGTCGCATATGAAGAACCCTC
mIars	TCGGGAAGTCATCAATCGCATC	TCAGTGTGGCTTTCAATGACA
mGars	GGAGGCAGCACTTTATCCAAG	TCGGAAGCACTCTCCGTTCT
mCol1a1	CGCCATCAAGGTCTACTGCAA	CTCGCTTCCGTACTCGAAC
mCol3a1	TAAAATTCTGCCACCCCGAAC	TGCACCAGAATCTGTCCAC
mLtbp2	AGCCTCCCAAATGGATACAGA	TGACCATGATGTAGCCCCGAT
RN18S	TGACTCAACACGGGAAACCTC	CATGCCAGAGTCTCGTTCGTT
Taqman probes		
Gene	**Assay ID.**	**Company**
hCOL1A1	Hs00164004_m1	ThermoFisher Scientific
hCOL3A1	Hs00943809_m1	ThermoFisher Scientific
hGAPDH	Hs02786624_g1	ThermoFisher Scientific
hACTB	Hs01060665_g1	ThermoFisher Scientific
RN18S	Mm03928990_g1	ThermoFisher Scientific
mNppa	Mm01255747_g1	ThermoFisher Scientific
mNppb	Mm01255770_g1	ThermoFisher Scientific
mMyh6	Mm00440359_m1	ThermoFisher Scientific
mMyh7	Mm01319006_g1	ThermoFisher Scientific
mGapdh	Mm99999915_g1	ThermoFisher Scientific
mActb	Mm00607939_s1	ThermoFisher Scientific
Genotyping primers		
Eprs-gKO	Forward: AAGCTGTGGTGTGCTTGTACTCA Reverse: CATCAGGTTAGTCCCATACAGCTG	
Eprs-Flox	Forward: TCCAAGCCTCTGTACTGAGTTC Reverse: AAGAGTCACAATGGCACAAACAG	
$Postn^{MCM}$	WT-Forward: TCTGTAAGGCCATCGCAAGCT Cre-Forward: TCTTGGCTCACTGCAATCTCC Com-Reverse: ATTTACAAGGAACTTCACGCA	

Online Table XII: Overall P values for comparisons among ≥3 groups.

Main figures		tests	Overall P value
Figure 2	Figure 2A	Kruskal-Wallis test with Conover-Iman post hoc pariwise comparisons	Overall P value: P=3.13E-4
	Figure 2B	Kruskal-Wallis test with Conover-Iman post hoc pariwise comparisons	Overall P value: P=1.83E-65
	Figure 2C	Kruskal-Wallis test with Conover-Iman post hoc pariwise comparisons	Overall P value: P=1.68E-4
	Figure 2D	Kruskal-Wallis test with Conover-Iman post hoc pariwise comparisons	Overall P value: P=5.79E-5
	Figure 2E	Kruskal-Wallis test with Conover-Iman post hoc pariwise comparisons	Overall P value: P=6.11E-284
	Figure 2F	Kruskal-Wallis test with Conover-Iman post hoc pariwise comparisons	Overall P value: P=0.0014
	Figure 2H	Kruskal-Wallis test with Conover-Iman post hoc pariwise comparisons	FS: Overall P value: P=1.24E-5
			EF: Overall P value: P=1.24E-5
Figure 3	Figure 3G	Kruskal-Wallis test with Conover-Iman post hoc pariwise comparisons	Overall P value: P=0.0066
	Figure 3H	Kruskal-Wallis test with Conover-Iman post hoc pariwise comparisons	Overall P value: P=0.0019
	Figure 3I	Kruskal-Wallis test with Conover-Iman post hoc pariwise comparisons	FS: Overall P value: P=0.0090
			EF: Overall P value: P=0.011
Figure 4	Figure 4B	Kruskal-Wallis test with Conover-Iman post hoc pariwise comparisons	Overall P value: P=0.0015
	Figure 4C	Kruskal-Wallis test with Conover-Iman post hoc pariwise comparisons	Overall P value: P=5.84E-4
	Figure 4D	Kruskal-Wallis test with Conover-Iman post hoc pariwise comparisons	EPRS-FLAG: Overall P value: P=0.026
			COL1A1: Overall P value: P=0.022
			COL3A1: Overall P value: P=0.027
			α-SMA: Overall P value: P=0.018
	Figure 4E	Kruskal-Wallis test with Conover-Iman post hoc pariwise comparisons	COL1A1: Overall P value: P=2.2E-16
			EPRS-FLAG: Overall P value: P=1.99E-138
	Figure 4F	Kruskal-Wallis test with Conover-Iman post hoc pariwise comparisons	Overall P value: P=2.46E-84
Figure 6	Figure 6F	Kruskal-Wallis test with Conover-Iman post hoc pariwise comparisons	Overall P value: P=0.0060
	Figure 6G	Kruskal-Wallis test with Conover-Iman post hoc pariwise comparisons	Overall P value: P=0.0013
	Figure 6H	Kruskal-Wallis test with Conover-Iman post hoc pariwise comparisons	Overall P value: P=8.24E-5
Figure 7	Figure 7A	Kruskal-Wallis test with Conover-Iman post hoc pariwise comparisons	Overall P value: P=0.0055
	Figure 7B	Kruskal-Wallis test with Conover-Iman post hoc pariwise comparisons	Sulf1: Overall P value: P=0.023
			Acta2: Overall P value: P=0.021
			Col1a1: Overall P value: P=0.016
			Postn: Overall P value: P=0.015
	Figure 7C	Kruskal-Wallis test with Conover-Iman post hoc pariwise comparisons	SULF1: Overall P value: P=1.17E-71
			COL1A1: Overall P value: P=2.39E-51
			α-SMA: Overall P value: P=5.22E-23
	Figure 7D	Kruskal-Wallis test with Conover-Iman post hoc pariwise comparisons	SULF1-FLAG: Overall P value: P=0.0053
			COL1A1: Overall P value: P=0.0051
			α-SMA: Overall P value: P=0.0028
	Figure 7E	Kruskal-Wallis test with Conover-Iman post hoc pariwise comparisons	SULF1: Overall P value: P=6.83E-213
Figure 7	Figure 7E	Kruskal-Wallis test with Conover-Iman post hoc pariwise comparisons	COL1A1: Overall P value: P=2.22E-154
			α-SMA: Overall P value: P=7.83E-157
Figure 8	Figure 8B	Kruskal-Wallis test with Conover-Iman post hoc pariwise comparisons	Overall p value: P=8.02E-119
	Figure 8C	Kruskal-Wallis test with Conover-Iman post hoc pariwise comparisons	Overall p value: P=4,60E-151
	Figure 8D	Kruskal-Wallis test with Conover-Iman post hoc pariwise comparisons	SULF1-FLAG: Overall P value: P=0.0011
			COL1A1: Overall P value: P=4.39E-4
			COL3A1: Overall P value: P=0.0058

			α-SMA: Overall P value: P=0.0044

Online figures		**tests**	**P value**
Online Figure II	Figure IIG	Kruskal-Wallis test with Conover-Iman post hoc pariwise comparisons	Overall p value: P=2.78E-120
Online Figure III	Figure IIIB	Kruskal-Wallis test with Conover-Iman post hoc pariwise comparisons	Overall P value: P=3.04E-13
Online Figure V	Figure VF	Kruskal-Wallis test with Conover-Iman post hoc pariwise comparisons	Top: Overall P value: P=0.0015
			Bottom: Overall P value: P=4.95E-4
	Figure VG	Kruskal-Wallis test with Conover-Iman post hoc pariwise comparisons	Overall P value: P=4.06E-79
Online Figure VII	Figure VIIC	Kruskal-Wallis test with Conover-Iman post hoc pariwise comparisons	Overall P value: P=0.0065
	Figure VIID	Kruskal-Wallis test with Conover-Iman post hoc pariwise comparisons	Overall P value: P=0.0079
Online Figure VIII	Figure VIIIC	Kruskal-Wallis test with Conover-Iman post hoc pariwise comparisons	Overall P value: P=0.0096
	Figure VIIID	Kruskal-Wallis test with Conover-Iman post hoc pariwise comparisons	Overall P value: P=0.0018
	Figure VIIIE	Kruskal-Wallis test with Conover-Iman post hoc pariwise comparisons	Overall P value: P=4.73E-4
Online Figure IX	Figure IXB	Kruskal-Wallis test with Conover-Iman post hoc pariwise comparisons	Overall P value: P=4.31E-22
	Figure IXF	Kruskal-Wallis test with Conover-Iman post hoc pariwise comparisons	Overall P value: P=1.67E-116
	Figure IXG	Kruskal-Wallis test with Conover-Iman post hoc pariwise comparisons	Overall P value: P=6.07E-116
Online Figure XII	Figure XIIA	Kruskal-Wallis test with Conover-Iman post hoc pariwise comparisons	Overall P value: P=8.97E-76
	Figure XIIB	Kruskal-Wallis test with Conover-Iman post hoc pariwise comparisons	Overall P value: P=2.51E-61
	Figure XIIC	Kruskal-Wallis test with Conover-Iman post hoc pariwise comparisons	Overall P value: P=0.066

Supplemental Sequence Information

Human COL1A1 protein sequence:

MFSFVDLRLLLLLAATALLTHGQEEGQVEGQDEDIPPITCVQNGLRYHDRDVWKPEPCRICVCDN
GKVLCDDVICDETKNCPGAEVPEGECCPVCPDGSESPTDQETTGVEGPKGDTGPRGPRGPAGPP
GRDGIPGQPGLPGPPGPPGPPGPPGLGGNFAPQLSYGYDEKSTGGISVPGPMGPSGPRGLPGP
PGAPGPQGFQGPPGEPGEPGASGPMGPRGPPGPPGKNGDDGEAGKPGRPGERGPPGPQGAR
GLPGTAGLPGMKGHRGFSGLDGAKGDAGPAGPKGEPGSPGENGAPGQMGPRGLPGERGRPG
APGPAGARGNDGATGAAGPPGPTGPAGPPGFPGAVGAKGEAGPQGPRGSEGPQGVRGEPGPP
GPAGAAGPAGNPGADGQPGAKGANGAPGIAGAPGFPGARGPSGPQGPGGPPGPKGNSGEPG
APGSKGDTGAKGEPGPVGVQGPPGPAGEEGKRGARGEPGPTGLPGPPGERGGPGSRGFPGAD
GVAGPKGPAGERGSPGPAGPKGSPGEAGRPGEAGLPGAKGLTGSPGSPGPDGKTGPPGPAGQ
DGRPGPPGPPGARGQAGVMGFPGPKGAAGEPGKAGERGVPGPPGAVGPAGKDGEAGAQGPP
GPAGPAGERGEQGPAGSPGFQGLPGPAGPPGEAGKPGEQGVPGDLGAPGPSGARGERGFPGE
RGVQGPPGPAGPRGANGAPGNDGAKGDAGAPGAPGSQGAPGLQGMPGERGAAGLPGPKGD
RGDAGPKGADGSPGKDGVRGLTGPIGPPGPAGAPGDKGESGPSGPAGPTGARGAPGDRGEPG
PPGPAGFAGPPGADGQPGAKGEPGDAGAKGDAGPPGPAGPAGPPGPIGNVGAPGAKGARGSA
GPPGATGFPGAAGRVGPPGPSGNAGPPGPPGPAGKEGGKGPRGETGPAGRPGEVGPPGPPGP
AGEKGSPGADGPAGAPGTPGPQGIAGQRGVVGLPGQRGERGFPGLPGPSGEPGKQGPSGASG
ERGPPGPMGPPGLAGPPGESGREGAPGAEGSPGRDGSPGAKGDRGETGPAGPPGAPGAPGA
PGPVGPAGKSGDRGETGPAGPAGPVGPVGARGPAGPQGPRGDKGETGEQGDRGIKGHRGFSG
LQGPPGPPGSPGEQGPSGASGPAGPRGPPGSAGAPGKDGLNGLPGPIGPPGPRGRTGDAGPV
GPPGPPGPPGPPGPPSAGFDFSFLPQPPQEKAHDGGRYYRADDANVVRDRDLEVDTTLKSLSQ
QIENIRSPEGSRKNPARTCRDLKMCHSDWKSGEYWIDPNQGCNLDAIKVFCNMETGETCVYPTQ
PSVAQKNWYISKNPKDKRHVWFGESMTDGFQFEYGGQGSDPADVAIQLTFLRLMSTEASQNITY
HCKNSVAYMDQQTGNLKKALLLQGSNEIEIRAEGNSRFTYSVTVDGCTSHTGAWGKTVIEYKTTK
TSRLPIIDVAPLDVGAPDQEFGFDVGPVCFL

Mouse COL1A1 protein sequence:

MFSFVDLRLLLLLGATALLTHGQEDIPEVSCIHNGLRVPNGETWKPEVCLICICHNGTAVCDDVQC
NEELDCPNPQRREGECCAFCPEEYVSPNSEDVGVEGPKGDPGPQGPRGPVGPPGRDGIPGQPG
LPGPPGPPGPPGPPGLGGNFASQMSYGYDEKSAGVSVPGPMGPSGPRGLPGPPGAPGPQGFQ
GPPGEPGEPGGSGPMGPRGPPGPPGKNGDDGEAGKPGRPGERGPPGPQGARGLPGTAGLPG
MKGHRGFSGLDGAKGDAGPAGPKGEPGSPGENGAPGQMGPRGLPGERGRPGPPGTAGARGN
DGAVGAAGPPGPTGPTGPPGFPGAVGAKGEAGPQGARGSEGPQGVRGEPGPPGPAGAAGPAG
NPGADGQPGAKGANGAPGIAGAPGFPGARGPSGPQGPSGPPGPKGNSGEPGAPGNKGDTGA
KGEPGATGVQGPPGPAGEEGKRGARGEPGPSGLPGPPGERGGPGSRGFPGADGVAGPKGPSG
ERGAPGPAGPKGSPGEAGRPGEAGLPGAKGLTGSPGSPGPDGKTGPPGPAGQDGRPGPAGPP
GARGQAGVMGFPGPKGTAGEPGKAGERGLPGPPGAVGPAGKDGEAGAQGAPGPAGPAGERG
EQGPAGSPGFQGLPGPAGPPGEAGKPGEQGVPGDLGAPGPSGARGERGFPGERGVQGPPGPA
GPRGNNGAPGNDGAKGDTGAPGAPGSQGAPGLQGMPGERGAAGLPGPKGDRGDAGPKGAD
GSPGKDGARGLTGPIGPPGPAGAPGDKGEAGPSGPPGPTGARGAPGDRGEAGPPGPAGFAGP
PGADGQPGAKGEPGDTGVKGDAGPPGPAGPAGPPGPIGNVGAPGPKGPRGAAGPPGATGFPG
AAGRVGPPGPSGNAGPPGPPGPVGKEGGKGPRGETGPAGRPGEVGPPGPPGPAGEKGSPGAD
GPAGSPGTPGPQGIAGQRGVVGLPGQRGERGFPGLPGPSGEPGKQGPSGSSGERGPPGPMGP
PGLAGPPGESGREGSPGAEGSPGRDGAPGAKGDRGETGPAGPPGAPGAPGAPGPVGPAGKNG
DRGETGPAGPAGPIGPAGARGPAGPQGPRGDKGETGEQGDRGIKGHRGFSGLQGPPGSPGSP
GEQGPSGASGPAGPRGPPGSAGSPGKDGLNGLPGPIGPPGPRGRTGDSGPAGPPGPPGPPGP
PGPPSGGYDFSFLPQPPQEKSQDGGRYYRADDANVVRDRDLEVDTTLKSLSQQIENIRSPEGSRK

NPARTCRDLKMCHSDWKSGEYWIDPNQGCNLDAIKVYCNMETGQTCVFPTQPSVPQKNWYISP
NPKEKKHVWFGESMTDGFPFEYGSEGSDPADVAIQLTFLRLMSTEASQNITYHCKNSVAYMDQQ
TGNLKKALLLQGSNEIELRGEGNSRFTYSTLVDGCTSHTGTWGKTVIEYKTTKTSRLPIIDVAPLDIG
APDQEFGLDIGPACFV

Human COL3A1 protein sequence:

MMSFVQKGSWLLLALLHPTIILAQQEAVEGGCSHLGQSYADRDVWKPEPCQICVCDSGSVLCDDI
ICDDQELDCPNPEIPFGECCAVCPQPPTAPTRPPNGQGPQGPKGDPGPPGIPGRNGDPGIPGQP
GSPGSPGPPGICESCPTGPQNYSPQYDSYDVKSGVAVGGLAGYPGPAGPPGPPGPPGTSGHPG
SPGSPGYQGPPGEPGQAGPSGPPGPPGAIGPSGPAGKDGESGRPGRPGERGLPGPPGIKGPA
GIPGFPGMKGHRGFDGRNGEKGETGAPGLKGENGLPGENGAPGPMGPRGAPGERGRPGLPGA
AGARGNDGARGSDGQPGPPGPPGTAGFPGSPGAKGEVGPAGSPGSNGAPGQRGEPGPQGHA
GAQGPPGPPGINGSPGGKGEMGPAGIPGAPGLMGARGPPGPAGANGAPGLRGGAGEPGKNG
AKGEPGPRGERGEAGIPGVPGAKGEDGKDGSPGEPGANGLPGAAGERGAPGFRGPAGPNGIPG
EKGPAGERGAPGPAGPRGAAGEPGRDGVPGGPGMRGMPGSPGGPGSDGKPGPPGSQGESG
RPGPPGPSGPRGQPGVMGFPGPKGNDGAPGKNGERGGPGGPGPQGPPGKNGETGPQGPPG
PTGPGGDKGDTGPPGPQGLQGLPGTGGPPGENGKPGEPGPKGDAGAPGAPGGKGDAGAPGE
RGPPGLAGAPGLRGGAGPPGPEGGKGAAGPPGPPGAAGTPGLQGMPGERGGLGSPGPKGDK
GEPGGPGADGVPGKDGPRGPTGPIGPPGPAGQPGDKGEGGAPGLPGIAGPRGSPGERGETGP
PGPAGFPGAPGQNGEPGGKGERGAPGEKGEGGPPGVAGPPGGSGPAGPPGPQGVKGERGSP
GGPGAAGFPGARGLPGPPGSNGNPGPPGPSGSPGKDGPPGPAGNTGAPGSPGVSGPKGDAG
QPGEKGSPGAQGPPGAPGPLGIAGITGARGLAGPPGMPGPRGSPGPQGVKGESGKPGANGLS
GERGPPGPQGLPGLAGTAGEPGRDGNPGSDGLPGRDGSPGGKGDRGENGSPGAPGAPGHPGP
PGPVGPAGKSGDRGESGPAGPAGAPGPAGSRGAPGPQGPRGDKGETGERGAAGIKGHRGFP
GNPGAPGSPGPAGQQGAIGSPGPAGPRGPVGPSGPPGKDGTSGHPGPIGPPGPRGNRGERGS
EGSPGHPGQPGPPGPPGAPGPCCGGVGAAAIAGIGGEKAGGFAPYYGDEPMDFKINTDEIMTSL
KSVNGQIESLISPDGSRKNPARNCRDLKFCHPELKSGEYWVDPNQGCKLDAIKVFCNMETGETCI
SANPLNVPRKHWWTDSSAEKKHVWFGESMDGGFQFSYGNPELPEDVLDVQLAFLRLLSSRASQ
NITYHCKNSIAYMDQASGNVKKALKLMGSNEGEFKAEGNSKFTYTVLEDGCTKHTGEWSKTVFEY
RTRKAVRLPIVDIAPYDIGGPDQEFGVDVGPVCFL

Mouse COL3A1 protein sequence:

MMSFVQSGTWFLLTLLHPTLILAQQSNVDELGCSHLGQSYESRDVWKPEPCQICVCDSGSVLCD
DIICDEEPLDCPNPEIPFGECCAICPQPSTPAPVLPDGHGPQGPKGDPGPPGIPGRNGDPGLPGQ
PGLPGPPGSPGICESCPTGGQNYSPQFDSYDVKSGVGGMGGYPGPAGPPGPPGPPGSSGHPG
SPGSPGYQGPPGEPGQAGPAGPPGPPGALGPAGPAGKDGESGRPGRPGERGLPGPPGIKGPA
GMPGFPGMKGHRGFDGRNGEKGETGAPGLKGENGLPGDNGAPGPMGPRGAPGERGRPGLPG
AAGARGNDGARGSDGQPGPPGPPGTAGFPGSPGAKGEVGPAGSPGSNGSPGQRGEPGPQGH
AGAQGPPGPPGNNGSPGGKGEMGPAGIPGAPGLIGARGPPGPAGTNGIPGTRGPSGEPGKNGA
KGEPGARGERGEAGSPGIPGPKGEDGKDGSPGEPGANGLPGAAGERGPSGFRGPAGPNGIPGE
KGPPGERGGPGPAGPRGVAGEPGRDGTPGGPGIRGMPGSPGGPGNDGKPGPPGSQGESGRP
GPPGPSGPRGQPGVMGFPGPKGNDGAPGKNGERGGPGGPGLPGPAGKNGETGPQGPPGPTG
PAGDKGDSGPPGPQGLQGIPGTGGPPGENGKPGEPGPKGEVGAPGAPGGKGDSGAPGERGPP
GTAGIPGARGGAGPPGPEGGKGPAGPPGPPGASGSPGLQGMPGERGGPGSPGPKGEKGEPG
GAGADGVPGKDGPRGPAGPIGPPGPAGQPGDKGEGGSPGLPGIAGPRGGPGERGEHGPPGPA
GFPGAPGQNGEPGAKGERGAPGEKGEGGPPGPAGPTGSSGPAGPPGPQGVKGERGSPGGPG
TAGFPGGRGLPGPPGNNGNPGPPGPSGAPGKDGPPGPAGNSGSPGNPGIAGPKGDAGQPGEK
GPPGAQGPPGSPGPLGIAGLTGARGLAGPPGMPGPRGSPGPQGIKGESGKPGASGHNGERGP
PGPQGLPGQPGTAGEPGRDGNPGSDGQPGRDGSPGGKGDRGENGSPGAPGAPGHPGPPGPV

GPSGKSGDRGETGPAGPSGAPGPAGARGAPGPQGPRGDKGETGERGSNGIKGHRGFPGNPGP
PGSPGAAGHQGAIGSPGPAGPRGPVGPHGPPGKDGTSGHPGPIGPPGPRGNRGERGSEGSPG
HPGQPGPPGPPGAPGPCCGGGAAAIAGVGGEKSGGFSPYYGDDPMDFKINTEEIMSSLKSVNG
QIESLISPDGSRKNPARNCRDLKFCHPELKSGEYWVDPNQGCKMDAIKVFCNMETGETCINASP
MTVPRKHWWTDSGAEKKHVWFGESMNGGFQFSYGPPDLPEDVVDVQLAFLRLLSSRASQNITY
HCKNSIAYMDQASGNVKKSLKLMGSNEGEFKAEGNSKFTYTVLEDGCTKHTGEWSKTVFEYQTR
KAMRLPIIDIAPYDIGGPDQEFGVDIGPVCFL

Human SULF1 protein sequence:
MKYSCCALVLAVLGTELLGSLCSTVRSPRFRGRIQQERKNIRPNIILVLTDDQDVELGSLQVMNKTR
KIMEHGGATFINAFVTTPMCCPSRSSMLTGKYVHNHNVYTNNENCSSPSWQAMHEPRTFAVYLN
NTGYRTAFFGKYLNEYNGSYIPPGWREWLGLIKNSRFYNYTVCRNGIKEKHGFDYAKDYFTDLITN
ESINYFKMSKRMYPHRPVMMVISHAAPHGPEDSAPQFSKLYPNASQHITPSYNYAPNMDKHWIM
QYTGPMLPIHMEFTNILQRKRLQTLMSVDDSVERLYNMLVETGELENTYIIYTADHGYHIGQFGLVK
GKSMPYDFDIRVPFFIRGPSVEPGSIVPQIVLNIDLAPTILDIAGLDTPPDVDGKSVLKLLDPEKPGNR
FRTNKKAKIWRDTFLVERGKFLRKKEESSKNIQQSNHLPKYERVKELCQQARYQTACEQPGQKW
QCIEDTSGKLRIHKCKGPSDLLTVRQSTRNLYARGFHDKDKECSCRESGYRASRSQRKSQRQFL
RNQGTPKYKPRFVHTRQTRSLSVEFEGEIYDINLEEEEELQVLQPRNIAKRHDEGHKGPRDLQASS
GGNRGRMLADSSNAVGPPTTVRVTHKCFILPNDSIHCERELYQSARAWKDHKAYIDKEIEALQDKI
KNLREVRGHLKRRKPEECSCSKQSYYNKEKGVKKQEKLKSHLHPFKEAAQEVDSKLQLFKENNR
RRKKERKEKRRQRKGEECSLPGLTCFTHDNNHWQTAPFWNLGSFCACTSSNNNTYWCLRTVNE
THNFLFCEFATGFLEYFDMNTDPYQLTNTVHTVERGILNQLHVQLMELRSCQGYKQCNPRPKNLD
VGNKDGGSYDLHRGQLWDGWEG

Mouse SULF1 protein sequence:
MKYSLWALLLAVLGTQLLGSLCSTVRSQRFRGRIQQERKNIRPNIILVLTDDQDVELGSLQVMNKT
RKIMEQGGATFTNAFVTTPMCCPSRSSMLTGKYVHNHNVYTNNENCSSPSWQAMHEPRTFAVY
LNNTGYRTAFFGKYLNEYNGSYIPPGWREWLGLIKNSRFYNYTVCRNGIKEKHGFDYAKDYFTDLI
TNESINYFKMSKRMYPHRPIMMVISHAAPHGPEDSAPQFSKLYPNASQHITPSYNYAPNMDKHWI
MQYTGPMLPIHMEFTNVLQRKRLQTLMSVDDSVERLYNMLVESGELDNTYIIYTADHGYHIGQFG
LVKGKSMPYDFDIRVPFFIRGPSIEPGSIVPQIVLNIDLAPTILDIAGLDSPSDVDGKSVLKLLDLEKPG
NRFRTNKKAKIWRDTFLVERGKFLRKKEESGKNIQQSNHLPKYERVKELCQQARYQTACEQPGQ
NWQCIEDTSGKLRIHKCKGPSDLLTVRQNARNLYSRGLHDKDKECHCRDSGYRSSRSQRKNQR
QFLRNKGTPKYKPRFVHTRQTRSLSVEFEGEIYDINLEEEELQVLPPRSIAKRHDEGHQGFIGHQAA
AGDIRNEMLADSNNAVGLPATVRVTHKCFILPNDTIHCERELYQSARAWKDHKAYIDKEIEVLQDKI
KNLREVRGHLKKRKPEECGCGDQSYYNKEKGVKRQEKLKSHLHPFKEAAAQEVDSKLQLFKEHR
RRKKERKEKKRQRKGEECSLPGLTCFTHDNNHWQTAPFWNLGSFCACTSSNNNTYWCLRTVNE
THNFLFCEFATGFLEYFDMNTDPYQLTNTVHTVERSILNQLHIQLMELRSCQGYKQCNPRPKSLDI
GAKEGGNYDPHRGQLWDGWEG

Human LTBP2 protein sequence:
MRPRTKARSPGRALRNPWRGFLPLTLALFVGAGHAQRDPVGRYEPAGGDANRLRRPGGSYPAA
AAAKVYSLFREQDAPVAGLQPVERAQPGWGSPRRPTEAEARRPSRAQQSRRVQPPAQTRRSTPL
GQQQPAPRTRAAPALPRLGTPQRSGAAPPTPPRGRLTGRNVCGGQCCPGWTTANSTNHCIKPV
CEPPCQNRGSCSRPQLCVCRSGFRGARCEEVIPDEEFDPQNSRLAPRRWAERSPNLRRSSAAG
EGTLARAQPPAPQSPPAPQSPPAGTLSGLSQTHPSQQHVGLSRTVRLHPTATASSQLSSNALPP
GPGLEQRDGTQQAVPLEHPSSPWGLNLTEKIKKIKIVFTPTICKQTCARGHCANSCERGDTTTLYS
QGGHGHDPKSGFRIYFCQIPCLNGGRCIGRDECWCPANSTGKFCHLPIPQPDREPPGRGSRPRA
LLEAPLKQSTFTLPLSNQLASVNPSLVKVHIHHPPEASVQIHQVAQVRGGVEEALVENSVETRPPP

WLPASPGHSLWDSNNIPARSGEPPRPLPPAAPRPRGLLGRCYLNTVNGQCANPLLELTTQEDCC
GSVGAFWGVTLCAPCPPRPASPVIENGQLECPQGYKRLNLTHCQDINECLTLGLCKDAECVNTR
GSYLCTCRPGLMLDPSRSRCVSDKAISMLQGLCYRSLGPGTCTLPLAQRITKQICCCSRVGKAW
GSECEKCPLPGTEAFREICPAGHGYTYASSDIRLSMRKAEEEELARPPREQGQRSSGALPGPAER
QPLRVVTDTWLEAGTIPDKGDSQAGQVTTSVTHAPAWVTGNATTPPMPEQGIAEIQEEQVTPSTD
VLVTLSTPGIDRCAAGATNVCGPGTCVNLPDGYRCVCSPGYQLHPSQAYCTDDNECLRDPCKGK
GRCINRVGSYSCFCYPGYTLATSGATQECQDINECEQPGVCSGGQCTNTEGSYHCECDQGYIMV
RKGHCQDINECRHPGTCPDGRCVNSPGSYTCLACEEGYRGQSGSCVDVNECLTPGVCAHGKCT
NLEGSFRCSCEQGYEVTSDEKGCQDVDECASRASCPTGLCLNTEGSFACSACENGYWVNEDGT
ACEDLDECAFPGVCPSGVCTNTAGSFSCKDCDGGYRPSPLGDSCEDVDECEDPQSSCLGGECK
NTVGSYQCLCPQGFQLANGTVCEDVNECMGEEHCAPHGECLNSHGSFFCLCAPGFVSAEGGTS
CQDVDECATTDPCVGGHCVNTEGSFNCLCETGFQPSPESGECVDIDECEDYGDPVCGTWKCEN
SPGSYRCVLGCQPGFHMAPNGDCIDIDECANDTMCGSHGFCDNTDGSFRCLCDQGFEISPSGW
DCVDVNECELMLAVCGAALCENVEGSFLCLCASDLEEYDAQEGHCRPRGAGGQSMSEAPTGDH
APAPTRMDCYSGQKGHAPCSSVLGRNTTQAECCCTQGASWGDACDLCPSEDSAEFSEICPSGK
GYIPVEGAWTFGQTMYTDADECVIFGPGLCPNGRCLNTVPGYVCLCNPGFHYDASHKKCEDHDE
CQDLACENGECVNTEGSFHCFCSPPLTLDLSQQRCMNSTSSTEDLPDHDIHMDICWKKVTNDVC
SEPLRGHRTTYTECCCQDGEAWSQQCALCPPRSSEVYAQLCNVARIEAEREAGVHFRPGYEYGP
GPDDLHYSIYGPDGAPFYNYLGPEDTVPEPAFPNTAGHSADRTPILESPLQPSELQPHYVASHPEP
PAGFEGLQAEECGILNGCENGRCVRVREGYTCDCFEGFQLDAAHMACVDVNECDDLNGPAVLCV
HGYCENTEGSYRCHCSPGYVAEAGPPHCTAKE

Mouse LTBP2 protein sequence:
MRAPTTARCSGCIRRVRWRGFLPLVLAVLMGTSHAQRDSIGRYEPASRDANRLWHPVGSHPAAA
AAKVYSLFREPDAPVPGLSPSEWNQPAQGNPGRLAEAEARRPPRTQQLRRVQPPVQTRRSHPR
GQQQIAARAAPSVARLETPQRPAAARRGRLTGRNVCGGQCCPGWTTSNSTNHCIKPVCQPPCQ
NRGSCSRPQVCICRSGFRGARCEEVIPEEEFDPQNARPVPRRSVERAPGPHRSSEARGSLVTRIQ
PLVPPPSPPPSRRLSQPWPLQQHSGPSRTVRRYPATGANGQLMSNALPSGLELRDSSPQAAHV
NHLSPPWGLNLTEKIKKIKVVFTPTICKQTCARGRCANSCEKGDTTTLYSQGGHGHDPKSGFRIYF
CQIPCLNGGRCIGRDECWCPANSTGKFCHLPVPQPDREPAGRGSRHRTLLEGPLKQSTFTLPLS
NQLASVNPSLVKVQIHHPPEASVQIHQVARVRGELDPVLEDNSVETRASRRPHGNLGHSPWASNS
IPARAGEAPRPPPVLSRHYGLLGQCYLSTVNGQCANPLGELTSQEDCCGSVGTFWGVTSCAPCP
PRPAFPVIENGQLECPQGYKRLNLSHCQDINECLTLGLCKDSECVNTRGSYLCTCRPGLMLDPSR
SRCVSDKAVSMQQGLCYRSLGSGTCTLPLVHRITKQICCCSRVGKAWGSTCEQCPLPGTEAFREI
CPAGHGYTYSSSDIRLSMRKAEEEELASPLREQTEQSTAPPPGQAERQPLRAATATWIEAETLPDK
GDSRAVQITTSAPHLPARVPGDATGRPAPSLPGQGIPESPAEEQVIPSSDVLVTHSPPDFDPCFAG
ASNICGPGTCVSLPNGYRCVCSPGYQLHPSQDYCTDDNECMRNPCEGRGRCVNSVGSYSCLCY
PGYTLVTLRDTQECQDIDECEQPGVCSGGRCSNTEGSYHCECDRGYIMVRKGHCQDINECRHPG
TCPDGRCVNSPGSYTCLACEEGYVGQSGSCVDVNECLTPGICTHGRCINMEGSFRCSCEPGYEV
TPDKKGCRDVDECASRASCPTGLCLNTEGSFTCSACQSGYWVNEDGTACEDLDECAFPGVCPT
GVCTNTVGSFSCKDCDRGYRPNPLGNRCEDVDECEGPQSSCRGGECKNTEGSYQCLCHQGFQ
LVNGTMCEDVNECVGEEHCAPHGECLNSLGSFFCLCAPGFASAEGGTRCQDVDECAATDPCPG
GHCVNTEGSFSCLCETGFQPSPDSGECLDIDECEDREDPVCGAWRCENSPGSYRCILDCQPGFY
VAPNGDCIDIDECANDTVCGNHGFCDNTDGSFRCLCDQGFETSPSGWECVDVNECELMMAVCG
DALCENVEGSFLCLCASDLEEYDAEEGHCRPRVAGAQRIPEVRTEDQAPSLIRMECYSEHNGGPP
CSQILGQNSTQAECCCTQGARWGKACAPCPSEDSVEFSQLCPSGQGYIPVEGAWTFGQTMYTD
ADECVLFGPALCQNGRCLNIVPGYICLCNPGYHYDASSRKCQDHNECQDLACENGECVNTEGSF
HCLCNPPLTLDLSGQRCVNSTSSTEDFPDHDIHMDICWKKVTNDVCSQPLRGHHTTYTECCCQD
GEAWSQQCALCPPRSSEVYAQLCNVARIEAERGAGIHFRPGYEYGPGLDDLPENLYGPDGAPFY

NYLGPEDTAPEPPFSNPASQPGDNTPVLEPPLQPSELQPHYLASHSEPLASFEGLQAEECGILNG
CENGRCVRVREGYTCDCFEGFQLDAAHMACVDVNECEDLNGPAALCAHGHCENTEGSYRCHC
SPGYVAEPGPPHCAAKE

Human CKAP4 protein sequence:
MPSAKQRGSKGGHGAASPSEKGAHPSGGADDVAKKPPPAPQQPPPPPAPHPQQHPQQHPQN
QAHGKGGHRGGGGGGGKSSSSSSASAAAAAAAASSSASCSRRLGRALNFLFYLALVAAAAFSG
WCVHHVLEEVQQVRRSHQDFSRQREELGQGLQGVEQKVQSLQATFGTFESILRSSQHKQDLTEK
AVKQGESEVSRISEVLQKLQNEILKDLSDGIHVVKDARERDFTSLENTVEERLTELTKSINDNIAIFTE
VQKRSQKEINDMKAKVASLEESEGNKQDLKALKEAVKEIQTSAKSREWDMEALRSTLQTMESDIY
TEVRELVSLKQEQQAFKEAADTERLALQALTEKLLRSEESVSRLPEEIRRLEEELRQLKSDSHGPKE
DGGFRHSEAFEALQQKSQGLDSRLQHVEDGVLSMQVASARQTESLESLLSKSQEHEQRLAALQG
RLEGLGSSEADQDGLASTVRSLGETQLVLYGDVEELKRSVGELPSTVESLQKVQEQVHTLLSQDQ
AQAARLPPQDFLDRLSSLDNLKASVSQVEADLKMLRTAVDSLVAYSVKIETNENNLESAKGLLDDL
RNDLDRLFVKVEKIHEKV

Mouse CKAP4 protein sequence:
MPSAKQRGSKGGHGAASPSDKGAHPSGGADDVAKKPPAAPQQPQPPAPHPPQHPQNQAHRG
GHRGRSSAATANASSASCSRRLGRVLNFLFYLSLVAAAAFSGWYVHHVLEEVQQVRRGHQDFSR
QRDELGQGLQGVEQKVQSLQATFGTFESLLRNSQHKQDLTEKAVKEGESELNRISEVLQKLQNEIL
KDLSDGIHVVKDARERDFTSLENTVEERLTELTKSINDNIAIFTDVQKRSQKEINEVKMKVASLEESK
GDRSQDVKTLKDAVKEVQASMMSRERDIEALKSSLQTMESDVYTEVRELVSLKQEQQAFKQAAD
SERLALQALTEKLLRSEESSSRLPEDIRRLEEELQQLKVGAHGSEEGAVFKDSKALEELQRQIEGLG
ARLQYVEDGVYSMQVASARHTESLESLLSKSQEYEQRLAMLQEHVGNLGSSSDLASTVRSLGET
QLALSSDLKELKQSLGELPGTVESLQEQVLSLLSQDQAQAEGLPPQDFLDRLSSLDNLKSSVSQV
ESDLKMLRTAVDSLVAYSVKIETNENNLESAKGLLDDLRNDLDRLFLKVEKIHEKI

Human IL-11 protein sequence:
MNCVCRLVLVVLSLWPDTAVAPGPPPGPPRVSPDPRAELDSTVLLTRSLLADTRQLAAQLRDKFP
ADGDHNLDSLPTLAMSAGALGALQLPGVLTRLRADLLSYLRHVQWLRRAGGSSLKTLEPELGTLQ
ARLDRLLRRLQLLMSRLALPQPPPDPPAPPLAPPSSAWGGIRAAHAILGGLHLTLDWAVRGLLLLK
TRL

Mouse IL-11 protein sequence:
MNCVCRLVLVVLSLWPDRVVAPGPPAGSPRVSSDPRADLDSAVLLTRSLLADTRQLAAQMRDKF
PADGDHSLDSLPTLAMSAGTLGSLQLPGVLTRLRVDLMSYLRHVQWLRRAGGPSLKTLEPELGA
LQARLERLLRRLQLLMSRLALPQAAPDQPVIPLGPPASAWGSIRAAHAILGGLHLTLDWAVRGLLL
LKTRL